Supporting Information

A Dynamic Covalent Approach to $[Pt_nL_{2n}]^{2n+}$ Cages

Quinn V. C. van Hilst,[a] Aston C. Pearcy,[a] Dr. Dan Preston,[b] Prof. L. James Wright,[c] Prof. Christian G. Hartinger,[c] Assoc. Prof. Heather J. L. Brooks,[d] Prof. James D. Crowley*[a]

[a]Department of Chemistry, University of Otago, PO Box 56, Dunedin 9054, New Zealand

[b]Research School of Chemistry, Australian National University, Canberra ACT 0200, Australia

[c]School of Chemical Sciences, University of Auckland, Private Bag 92019, Auckland 1142, New Zealand

[d]Department of Pathology, University of Otago, PO Box 56, Dunedin 9054, New Zealand

*jcrowley@chemistry.otago.ac.nz

Contents

1 General Experimental Information

Unless otherwise stated, all reagents were purchased from commercial sources and used without further purification. *cis*-[$Pt(DMSO)_2(Cl)_2$] was prepared following literature methods.[1] Solvents were of laboratory reagent grade. Petroleum ether (petrol) refers to the fraction boiling in the range of 40-60 °C. Abbreviations for chemicals are as follows: methanol (MeOH), dichloromethane (DCM), chloroform ($CHCl_3$), dimethyl sulfoxide (DMSO), dimethylformamide (DMF), acetonitrile (MeCN), ethanol (EtOH), water (H_2O) and ethyl acetate (EtOAc). ^1H and $^{13}C\{^1H\}$ NMR spectra were recorded on either a 400 MHz Varian 400 MR®, a JEOL ECZ500R_S1 500 MHz NMR system retrofitted to a Varian 500 AR magnet or a JEOL ECZ600R_S1 600 MHz NMR system with a Jastec JMTC 600/54/JJ Magnet. Chemical shifts are reported in parts per million and referenced to residual solvent peaks ($CDCl_3$: ^1H δ 7.26 ppm, ^{13}C δ 77.16 ppm; MeCN-d_3: ^1H δ 1.94, ^{13}C δ 1.32, 118.26 ppm, DMSO-d_6: ^1H δ 2.50 ppm; ^{13}C δ 39.52 ppm; DMF-d_7: ^1H δ 8.03 ppm, ^{13}C δ 163.15 ppm, D_2O: ^1H δ 4.79 ppm). Coupling constants (*J*) are reported in Hertz (Hz). Standard abbreviations indicating multiplicity were used as follows: m = multiplet, td = triplet of doublets, t = triplet, quin = quintet, dt = doublet of triplets, d = doublet, dd = doublet of doublets, ddd = doublet of doublet of doublets, s = singlet, br = broad. IR spectra were recorded on a Bruker ALPHA FT-IR spectrometer with an attached ALPHA-P measurement module. Microanalyses were performed at the Campbell Microanalytical Laboratory at the University of Otago. Electrospray ionisation mass spectra (ESIMS) were collected on a Shimadzu LCMS-9030 spectrometer and a Bruker micro-TOF-Q spectrometer. Were necessary, spectra were obtained using pseudo-coldspray conditions (nebuliser (3.0 L/min) and heating gases (10.0 L/min) at room temperature, interface voltage = 3.50 kV, interface temperature = 373 K). UV-visible absorption spectra were acquired with a Shimadzu UV-2600 spectrophotometer. All ^1H DOSY NMR spectra were obtained using the convection compensated dstebpgp3s pulse sequence within Topspin.[2] The spectra were obtained with δ = 2.8 ms, Δ = 100 ms, and g = 2% – 95%. Data were analysed and visualised using MestReNova 14.2.2-29241, using the peak height method.

2 Experimental Procedures

2.1 Synthesis of $L_{4,4'}$

$L_{4,4'}$ was synthesised using a modified literature procedure.[3]

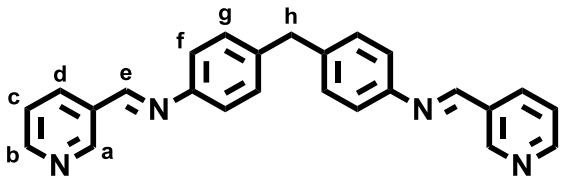

3-Pyridinecarboxaldehyde (0.099 mL, 2.1 mmol, 2.05 eq) was combined with 4,4'-diaminodiphenylmethane (0.102, 0.512 mmol, 1.0 eq) in MeOH (10 mL) and the resulting solution was heated under reflux for 4 h. The solution was cooled to RT and the product precipitated with diethyl ether (20 mL) and petrol (20 mL), collected via filtration and dried under vacuum to afford the **$L_{4,4'}$** as a yellow-cream coloured solid. Yield: 0.118 mg, 0.314 mmol, 61%. ^{1}H NMR (400 MHz, MeCN-d_3) δ: 9.01 (d, J = 2.1 Hz, 2H, H_a), 8.67 (dd, J = 4.8, 1.7 Hz, 2H, H_d), 8.61 (s, 2H, H_e), 8.26 (dt, J = 7.9, 2.0 Hz, 2H, H_d), 7.47 (dd, J = 7.9, 4.8 Hz, 2H, H_c), 7.32 (d, J = 8.3 Hz, 4H, H_f), 7.23 (d, J = 8.3 Hz, 4H, H_g), 4.03 (s, 2H, H_h).

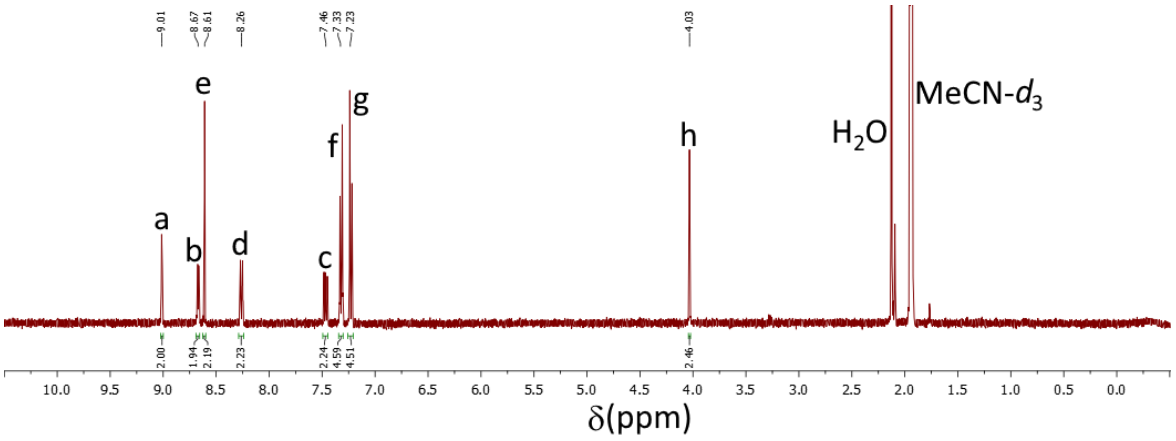

Figure S1: ^{1}H NMR spectrum (400 MHz, MeCN-d_3, 298 K) of **$L_{4,4'}$**.

2.2 Synthesis of L_{pxy}

L_{pxy} has been previously synthesised but was made using a modified literature procedure.[3-4]

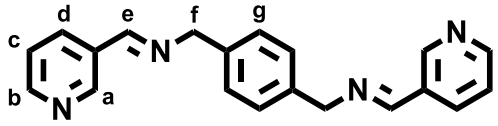

3-Pyridinecarboxaldehyde (0.141 mL, 1.51 mmol, 2.05 eq) was combined with *p*-xylylenediamine (0.100, 0.732 mmol, 1.0 eq) in MeOH (10 mL) and refluxed for 4 h. The solution was cooled to RT and the product precipitated with diethyl ether (20 mL) and petrol (20 mL), collected via filtration and dried under vacuum to afford the product as a cream coloured solid. Yield: 0.194 mg, 0.618 mmol, 84%. ^{1}H NMR (400 MHz, MeCN-d_3) δ: 8.89 (s, 2H, H_a), 8.62 (dd, J = 4.8, 1.7 Hz, 2H, H_b), 8.50 (s, 2H, H_e), 8.12 (dt, J = 7.9, 2.0 Hz, 2H, H_d), 7.40 (dd, J = 4.9, 2.9 Hz, 2H, H_c), 7.34 (s, 4H, H_g), 4.80 (s, 4H, H_f).

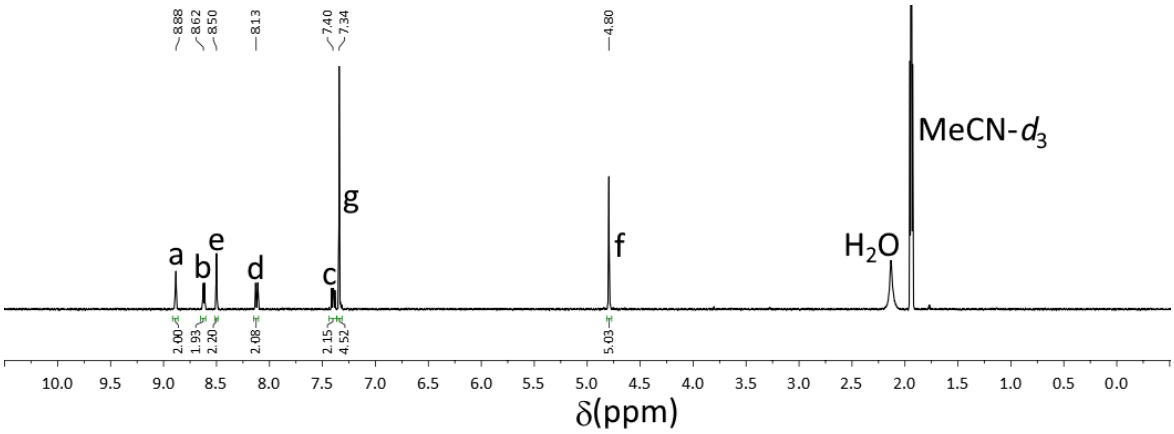

Figure S2: ^{1}H NMR spectrum (400 MHz, MeCN-d_3, 298 K) of **L_{pxy}**.

2.3 Synthesis of 2,6-dipicolinic acid dimethyl ester

2,6-dipicolinic acid dimethyl ester was synthesised using a modified literature procedure.[5]

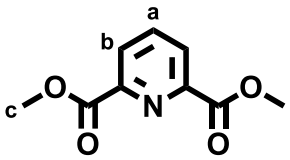

2,6-Dipicolinic acid (9.99 g, 59.8 mmol, 1.0 eq) was dissolved in MeOH (60 mL) and concentrated H_2SO_4 (3.32 mL) was added dropwise to the solution. The solution was stirred at reflux for 16 h, before being cooled to RT and then concentrated under

reduced pressure. The crude product was then dissolved in ethyl acetate (300 mL) and washed with H_2O (2×100 mL), saturated aqueous $NaHCO_3$ (50 mL) solution, and brine. The organic layer was dried over Na_2SO_4, filtered and the solvent removed *in vacuo* to afford the product as a white powder. Yield: 9.93 g, 50.8 mmol, 85%. ^{1}H NMR (400 MHz, $CDCl_3$) δ: 8.31 (d, J = 7.8 Hz, 2H, H_b), 8.02 (t, J = 7.6 Hz, 1H, H_a), 4.02 (s, 6H, H_c).

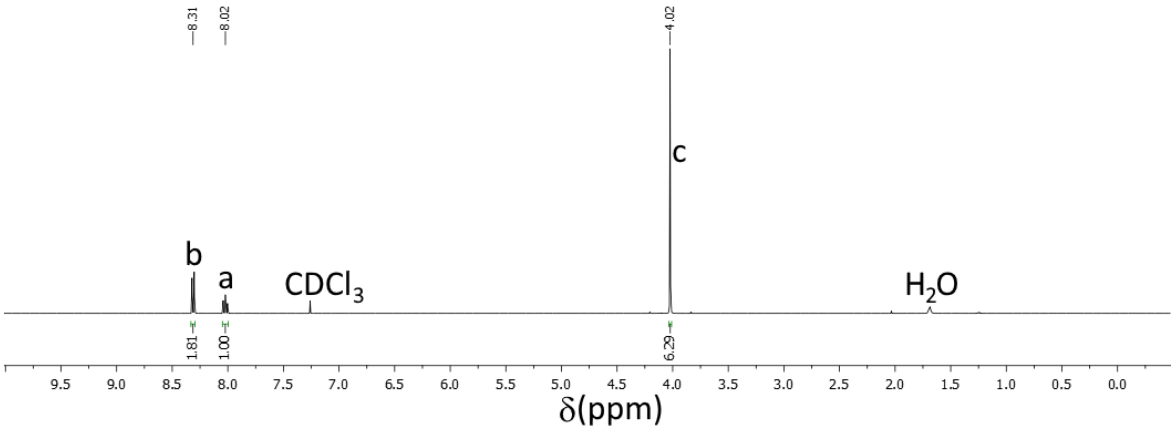

Figure S3: ^{1}H NMR spectrum (400 MHz, $CDCl_3$, 298 K) of 2,6-dipicolinic acid dimethyl ester.

2.4 Synthesis of isophthalic dihydrazide

Isophthalic dihydrazide was synthesised using a modified literature procedure.[6]

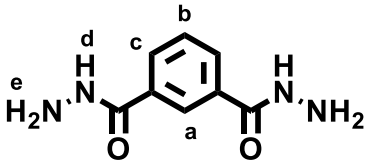

Dimethyl isophthalate (0.902 g, 18.0 mmol, 1.0 eq.) was dissolved in MeOH (60 mL) before hydrazine hydrate (10 mL, 40.0 eq.) was pipetted into the solution and the resulting mixture stirred at reflux for 17 h. After cooling to RT, the precipitate was collected via filtration and washed with EtOH (20 mL) and diethyl ether (20 mL) before being dried *in vacuo* to obtain the product as a white powder. Yield: 0.66 g, 3.40 mmol, 66%. ^{1}H NMR (400 MHz, DMSO-d_6) δ: 9.80 (s, 2H, H_d), 8.25 (t, J = 1.8 Hz, 1H, H_a), 7.91 (dd, J = 7.7, 1.7 Hz, 2H, H_c), 7.52 (t, J = 7.7 Hz, 1H, H_b), 4.52 (s, 4H, H_e). IR (ATR): ν (cm^{-1}) 3285, 3218, 3056, 1655, 1620, 1585, 1520, 1478, 1305, 1108, 995, 684, 616, 469.

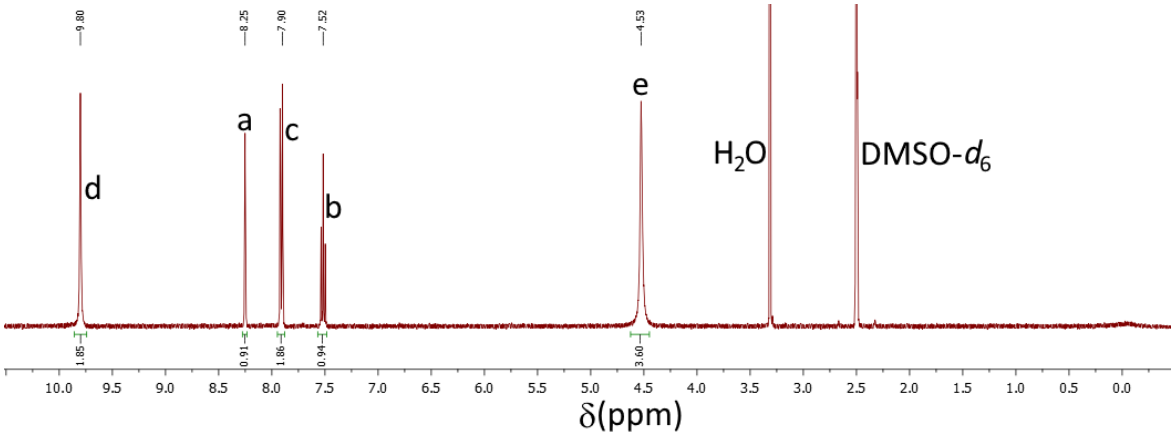

Figure S4: ^{1}H NMR spectrum (400 MHz, DMSO-d_6, 298 K) of isophthalic dihydrazide.

2.5 Synthesis of $[Pt(3\text{-py})_4](BF_4)_2$ ($[Pt(3\text{-pyridinecarboxaldehyde})_4](BF_4)_2$)

$[Pt(3\text{-pyridinecarboxaldehyde})_4](BF_4)_4$ was synthesised using a literature procedure.[7]

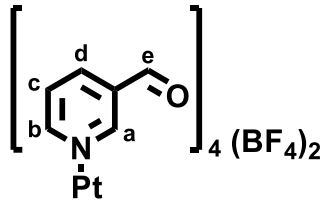

3-Pyridinecarboxaldehyde (0.270 mL, 2.88 mmol, 4.0 eq.) was stirred with $[Pt(DMSO)_2(Cl)_2]$ (0.299 g, 0.708 mmol, 1.0 eq.) and $AgBF_4$ (0.414 g, 2.13 mmol, 3.0 eq.) in MeCN (10 mL) at 60 °C for 18 h. The resulting reaction mixture was centrifuged and the supernatant collected and dried under vacuum. The product was washed with ether and dichloromethane to afford a white solid. Yield: 0.464 g, 0.582 mmol, 82%. ^{1}H NMR (400 MHz, DMSO-d_6) δ: 10.00 (s, 4H, H_e), 9.65 (d, J = 1.7 Hz, 4H, H_a), 9.39 (d, J = 5.9 Hz, 4H, H_b), 8.48 (dt, J = 7.9, 1.6 Hz, 4H, H_d), 7.91 (dd, J = 7.8, 5.7 Hz, 4H, H_c). IR (ATR): v (cm^{-1}) 3623, 3540, 3121, 3080, 3050, 1724, 1702, 1638, 1616, 1582, 1484, 1399, 1220, 1036, 1012, 857, 817, 691, 660, 520, 506.

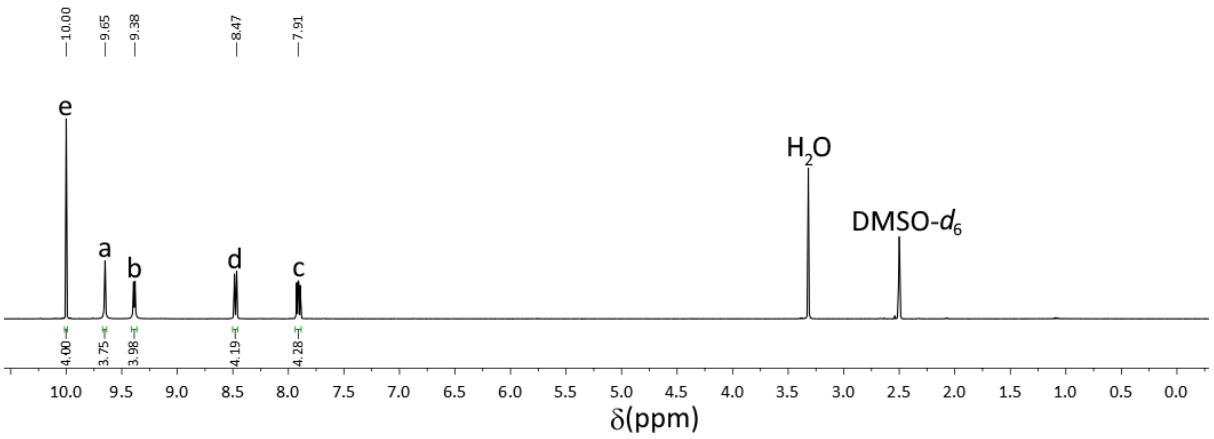

Figure S5: ^{1}H NMR spectrum (400 MHz, DMSO-d_6, 298 K) of [Pt(3-pyridinecarboxaldehyde)$_4$](BF$_4$)$_2$.

2.6 Synthesis of $Pd_{4,4}$

[Pd$_2$(L$_1$)$_4$](BF$_4$)$_4$ was synthesised using a modified literature procedure.[8]

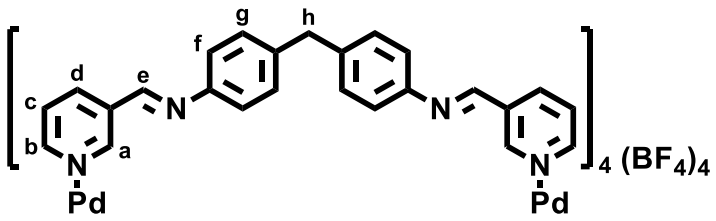

3-Pyridinecarboxaldehyde (37.5 µL, 0.400 mmol, 8.0 eq.), [Pd(MeCN)$_4$](BF$_4$)$_2$ (0.047 g, 0.105 mmol, 2.0 eq.) and 4,4′-diaminodiphenylmethane (0.042 g, 0.209 mmol, 4.0 eq.) were dissolved in DMSO (5 mL) and stirred at room temperature for 2 h. Ethyl acetate (40 mL) was added to the solution and the precipitate collected via centrifugation. The solid was washed with DCM and diethyl ether before drying *in vacuo* to afford the product as a pale yellow solid. Yield: 0.093 g, 0.045 mmol, 90%. ^{1}H NMR (400 MHz, DMSO-d_6) δ 10.10 (s, 8H, H$_a$), 9.41 (dd, *J* = 5.8, 1.4 Hz, 8H, H$_b$), 8.60 (s, 8H, H$_e$), 8.39 (dt, *J* = 8.1, 1.5 Hz, 8H, H$_d$), 7.89 (dd, *J* = 7.9, 5.7 Hz, 8H, H$_c$), 7.30 (d, *J* = 8.3 Hz, 16H, H$_f$), 7.20 (d, *J* = 8.3 Hz, 16H, H$_g$), 4.05 (s, 8H, H$_h$). Anal. calc. for C$_{100}$H$_{80}$N$_{16}$Pd$_2$B$_4$F$_{16}$•4(H$_2$O): C, 56.18%; H, 4.15%; N, 10.48%. Found: C, 56.26%; H, 3.82%; N, 10.50%. HR ESI MS (MeOH) *m/z* = 429.6211 [M – 4BF$_4$]$^{4+}$ (calc. for [C$_{100}$H$_{80}$N$_{16}$Pd$_2$]$^{4+}$, 429.6211), 601.8298 [M – 3BF$_4$]$^{3+}$ (calc. for [C$_{100}$H$_{80}$N$_{16}$Pt$_2$BF$_4$]$^{3+}$, 601.8295), 946.2466 [M – 2BF$_4$]$^{2+}$ (calc. for [C$_{100}$H$_{80}$N$_{16}$Pt$_2$B$_2$F$_8$]$^{2+}$, 946.2464).

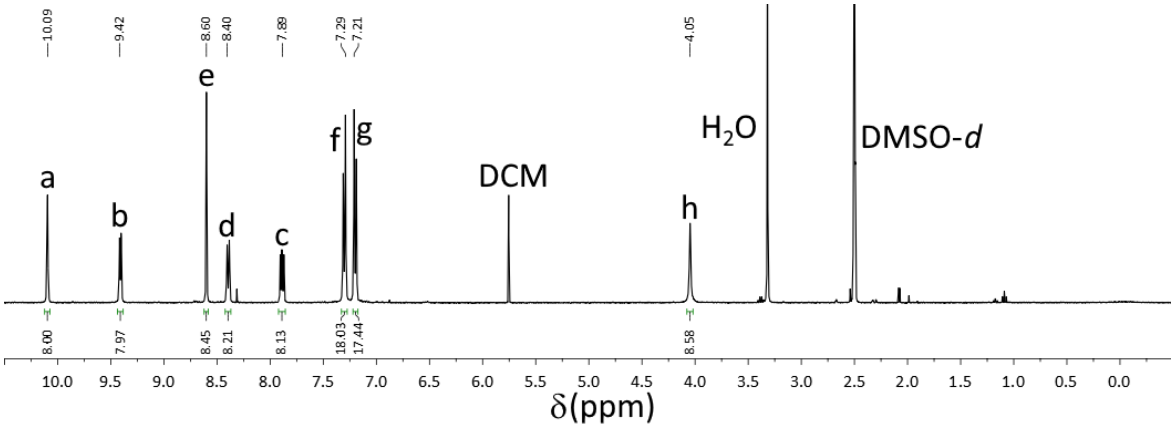

Figure S6: ^{1}H NMR spectrum (400 MHz, DMSO-d_6, 298 K) of **Pd$_{4,4'}$**.

2.7 Synthesis of $C_{4,4'}$

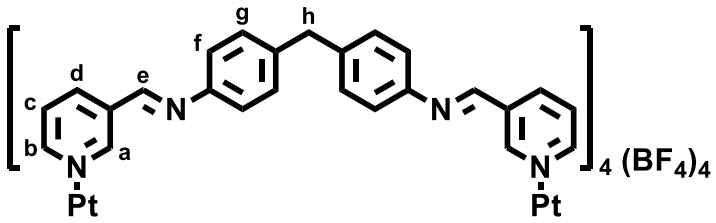

[Pt(3-pyridinecarboxaldehyde)$_4$](BF_4)$_2$ (0.080 g, 0.10 mmol, 2.0 eq.) and 4,4'-diaminodiphenylmethane (0.040 g, 0.20 mmol, 4.1 eq.) were dissolved in DMSO (10 mL) and stirred at RT for 18 h. Ethyl acetate (40 mL) was added to the solution and the resulting precipitate collected via centrifugation. The solid was washed with DCM and diethyl ether before drying *in vacuo* to afford the product as a pale yellow solid. Yield: 0.107 g, 0.048 mmol, 95%. ^{1}H NMR (400 MHz, DMSO-d_6) δ: 10.04 (s, 8H, H_a), 9.35 (d, J = 5.7 Hz, 8H, H_b), 8.61 (s, 8H, H_e), 8.41 (d, J = 8.1 Hz, 8H, H_d), 7.88 (dd, J = 7.8, 6.0 Hz, 8H, H_c), 7.29 (d, J = 8.4 Hz, 16H, H_f), 7.19 (d, J = 8.2 Hz, 16H, H_g), 4.05 (s, 8H, H_h). ^{13}C{^{1}H} NMR (100 MHz, DMSO-d$_6$) δ: 156.7, 152.9, 150.1, 148.6, 141.6, 140.0, 134.9, 129.7, 127.8, 121.1, 40.4. HR ESI MS (MeCN) *m/z* = 473.9036 [M – 4BF_4]$^{4+}$ (calc. for [$C_{100}H_{80}N_{16}Pt_2$]$^{4+}$, 473.9012), 1034.3059 [M – 2BF_4]$^{2+}$ (calc. for [$C_{100}H_{80}N_{16}Pt_2B_2F_8$]$^{2+}$, 1034.3102. Anal. calc. for $C_{100}H_{80}N_{16}Pt_2B_4F_{16}$•3(DMSO)•4($H_2O$): C, 49.93%; H, 4.19%; N, 8.79%. Found: C, 49.82%; H, 3.85%; N, 8.84%. IR (ATR): ν (cm^{-1}) 3591, 3102, 1630, 1604, 1501, 1438, 1062, 1015, 821, 698, 673, 659, 521.

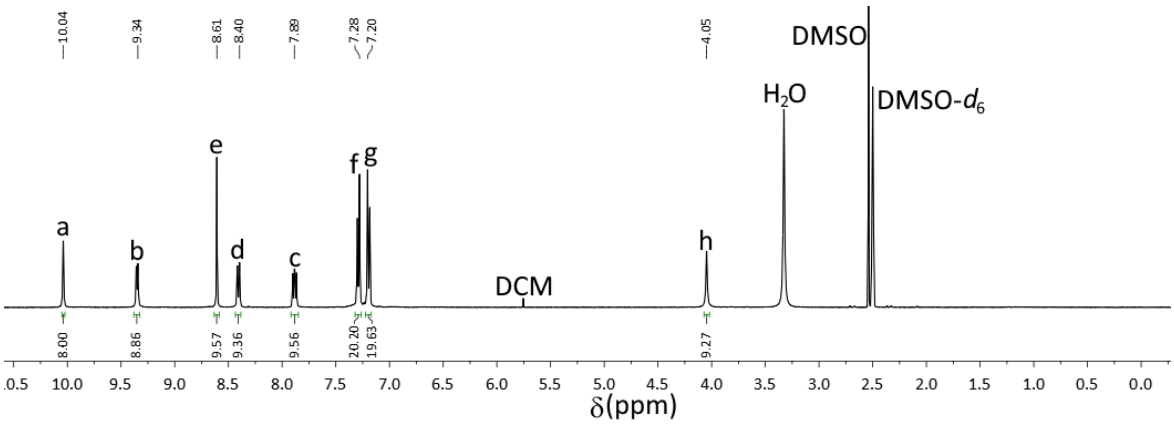

Figure S7: ^{1}H NMR spectrum (400 MHz, DMSO-d_6, 298 K) of **$C_{4,4'}$**.

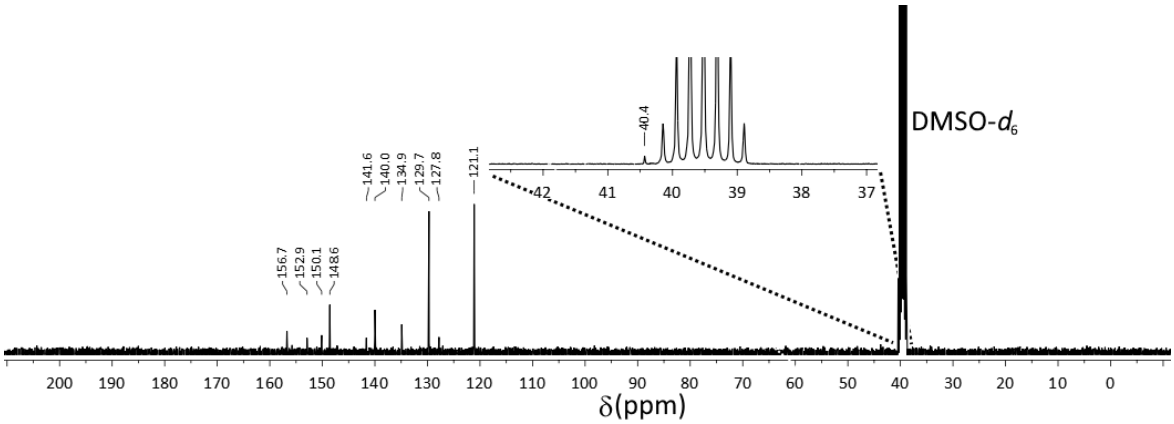

Figure S8: ^{13}C{^{1}H} NMR spectrum (100 MHz, DMSO-d_6, 298 K) of **$C_{4,4'}$**.

2.8 Synthesis of C_{nap}

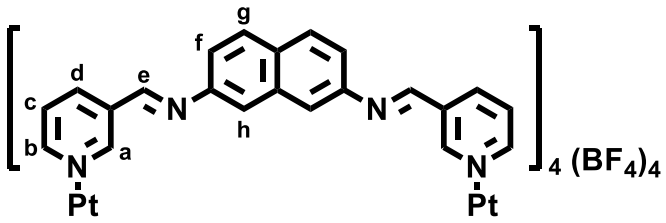

Pt(3-pyridinecarboxaldehyde)$_4$](BF$_4$)$_2$ (0.079 g, 0.099 mmol, 2.0 eq.) and 2,7-diaminonaphthalene (0.034 g, 0.21 mmol, 4.3 eq.) were dissolved in MeCN (10 mL) and stirred at 80 °C for 18 h. Diethyl ether (20 mL) was added to the solution and the resulting precipitate collected via centrifugation, washed with DCM once and dried *in vacuo* to afford the product as a brown solid. Yield: 0.077 g, 0.037 mmol, 74%. ^{1}H NMR (400 MHz, MeCN-d_3) δ 9.97 (s, 8H, H$_a$), 9.16 (d, J = 5.4 Hz, 8H, H$_b$), 8.95 (s, 8H, H$_e$), 8.44 (d, J = 7.9 Hz, 8H, H$_d$), 8.18 (s, 8H, H$_h$), 7.93 (d, J = 8.7 Hz, 8H, H$_f$), 7.75 (dd, J = 8.0, 5.8 Hz, 8H, H$_c$), 7.58 (dd, J = 8.7, 1.9 Hz, 8H, H$_g$). ^{13}C{^{1}H} NMR (100 MHz, DMSO-d_6) δ: 156.3, 153.0, 150.5, 146.7, 141.3, 135.3, 134.0, 131.9, 129.3, 128.0, 123.4, 119.0. HR ESI MS (MeCN) m/z = 433.8659 [M – 4BF$_4$]$^{4+}$ (calc. for

$[C_{88}H_{64}N_{16}Pt_2]^{4+}$, 433.8698), 607.4928 $[M - 3BF_4]^{3+}$ (calc. for $[C_{88}H_{64}N_{16}Pt_2BF_4]^{3+}$, 607.1607), 954.2404 $[M - 2BF_4]^{2+}$ (calc. for $[C_{88}H_{64}N_{16}Pt_2B_2F_8]^{2+}$, 954.2432). Anal. calc. for $C_{88}H_{64}N_{16}Pt_2B_4F_{16}\bullet 2CH_2Cl_2$: C, 47.98%; H, 3.04%; N, 9.95%. Found: C, 48.06%; H, 3.12%; N, 9.81%. IR (ATR): v (cm^{-1}) 3650, 3377, 3091, 1702, 1618, 1509, 1438, 1048, 901, 839, 812, 694, 519, 470.

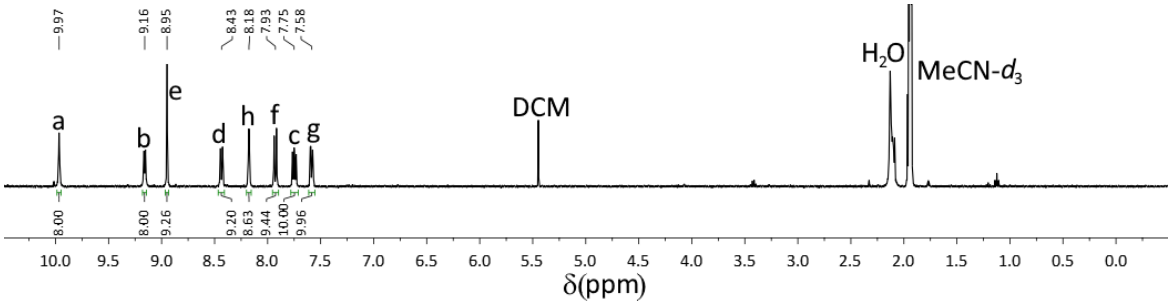

Figure S9: ^{1}H NMR spectrum (400 MHz, MeCN-d_3, 298 K) of $\mathbf{C_{nap}}$.

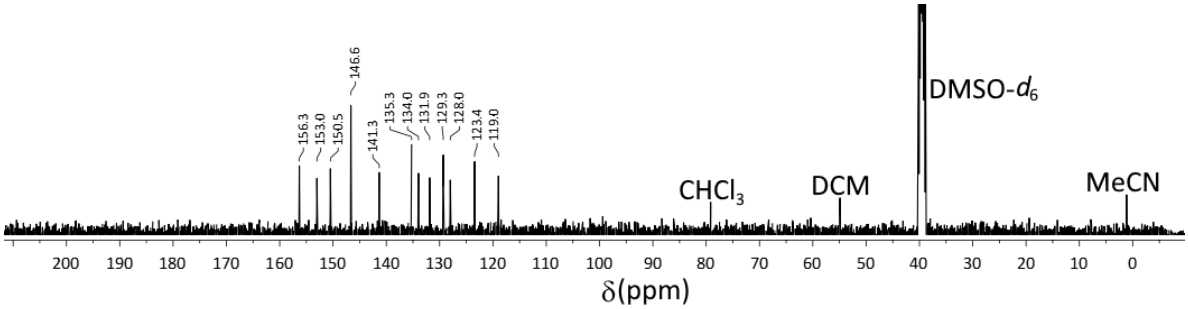

Figure S10: $^{13}C\{^{1}H\}$ NMR spectrum (100 MHz, DMSO-d_6, 298 K) of $\mathbf{C_{nap}}$.

2.9 Synthesis of C_{pxy}

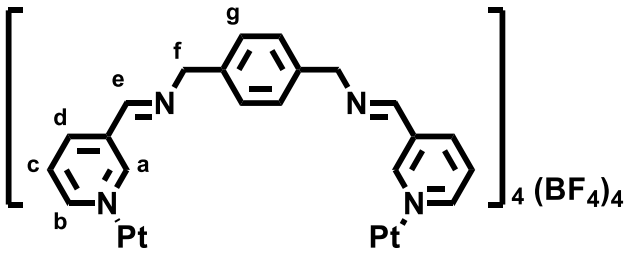

$[Pt(3\text{-pyridinecarboxaldehyde})_4](BF_4)_2$ (0.040 g, 0.051 mmol, 2.02 eq.) and *p*-xylylenediamine (0.015 g, 0.11 mmol, 4.38 eq.) were dissolved in MeCN (7.5 mL) and stirred at 60 °C for 18 h. Diethyl ether (20 mL) was added to the solution and the resulting precipitate collected via centrifugation, washed with DCM and dried *in vacuo* to afford the product as an off-white solid. Yield: 0.062 g, 0.031mmol, 61%. ^{1}H NMR (400 MHz, DMSO-d_6) δ 9.95 (s, 8H, H_a), 9.38 (d, J = 5.7 Hz, 8H, H_b), 8.56 (s, 8H, H_e), 8.25 (d, J = 7.9 Hz, 8H, H_d), 7.87 (dd, J = 7.4, 6.1 Hz, 8H, H_c), 7.36 (s, 16H, H_g), 4.89 (s, 16H, H_f). $^{13}C\{^{1}H\}$ NMR (100 MHz, DMSO-d_6) δ: 159.6, 152.5, 148.9, 142.3, 137.7, 134.7, 127.9, 127.5, 63.8. Pseudo-cryo ESI MS (MeCN) m/z = 411.8859 [M –

$4BF_4]^{4+}$ (calc. for $[C_{80}H_{72}N_{16}Pt_2]^{4+}$, 411.8854), 577.8485 $[M - 3BF_4]^{3+}$ (calc. for $[C_{80}H_{72}N_{16}Pt_2BF_4]^{3+}$, 577.8481), 910.2747 $[M - 2BF_4]^{2+}$ (calc. for $[C_{80}H_{72}N_{16}Pt_2B_2F_8]^{2+}$, 910.2745). Anal. calc. for $C_{80}H_{72}N_{16}Pt_2B_4F_{16}$•$5.5H_2O$: C, 45.51%; H, 3.68%; N, 10.63%. Found: C, 45.77%; H, 3.52%; N, 10.62%. IR (ATR): ν (cm^{-1}) 3612, 3095, 2858, 1700, 1645, 1610, 1591, 1514, 1439, 1054, 814, 695, 520.

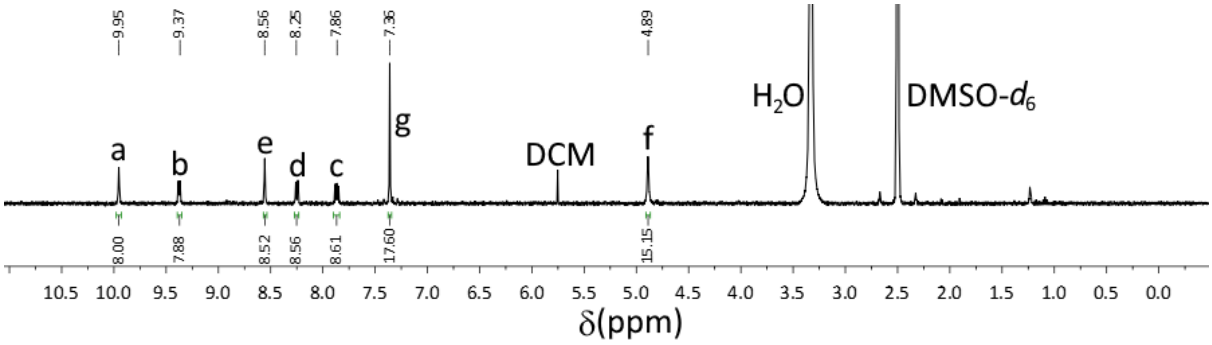

Figure S11: ^{1}H NMR spectrum (400 MHz, DMSO-d_6, 298 K) of $\mathbf{C_{pxy}}$.

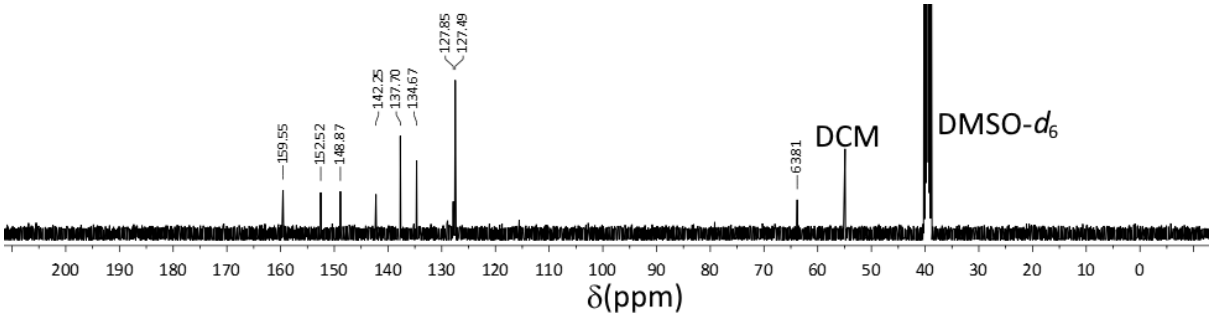

Figure S12: $^{13}C\{^1H\}$ NMR spectrum (100 MHz, DMSO-d_6, 298 K) of $\mathbf{C_{pxy}}$.

2.10 Synthesis of $\mathbf{C_{butyl}}$

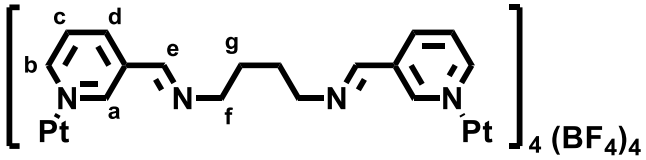

[Pt(3-pyridinecarboxaldehyde)$_4$]$(BF_4)_2$ (0.109 g, 0.137 mmol, 2.0 eq.) was dissolved in MeCN (20 mL) to which 1,4-diaminobutane (0.027 mL, 0.28 mmol, 4.0 eq) was added and the mixture was stirred at RT for 18 h. Diethyl ether (30 mL) was added to the solution and the resulting precipitate collected via centrifugation and dried *in vacuo* to afford the product as an off-white solid. Yield: 0.097 g, 0.054 mmol, 78%. ^{1}H NMR (400 MHz, DMSO-d_6) δ: 9.28 (s, 8H, H_a), 9.10 (d, J = 5.8 Hz, 8H, H_b), 8.44 – 8.32 (m, 16H, H_d/H_e), 7.83 (dd, J = 8.0, 5.9 Hz, 8H, H_c), 3.62 (br. s, 2H, H_f), 1.70 (broad s, 2H, H_g). Due to the low solubility of $\mathbf{C_{butyl}}$, a ^{13}C NMR spectrum was unable to be acquired. HR ESI MS (MeCN) *m/z* = 513.8499 $[M - 3BF_4]^{3+}$ (calc. for

$[C_{64}H_{72}N_{16}Pt_2BF_4]^{3+}$, 513.8481), 788.7579 [M – $2BF_4$ + Cl]$^{2+}$ (calc. for $[C_{64}H_{72}N_{16}Pt_2BF_4Cl]^{2+}$, 788.7570), 814.2749 [M – $2BF_4$]$^{2+}$ (calc. for $[C_{64}H_{72}N_{16}Pt_2B_2F_8]^{2+}$, 814.2743). IR (ATR): ν (cm^{-1}) 3604, 3109, 2923, 2857, 1647, 1610, 1439, 1377, 1324, 1051, 818, 697, 520.

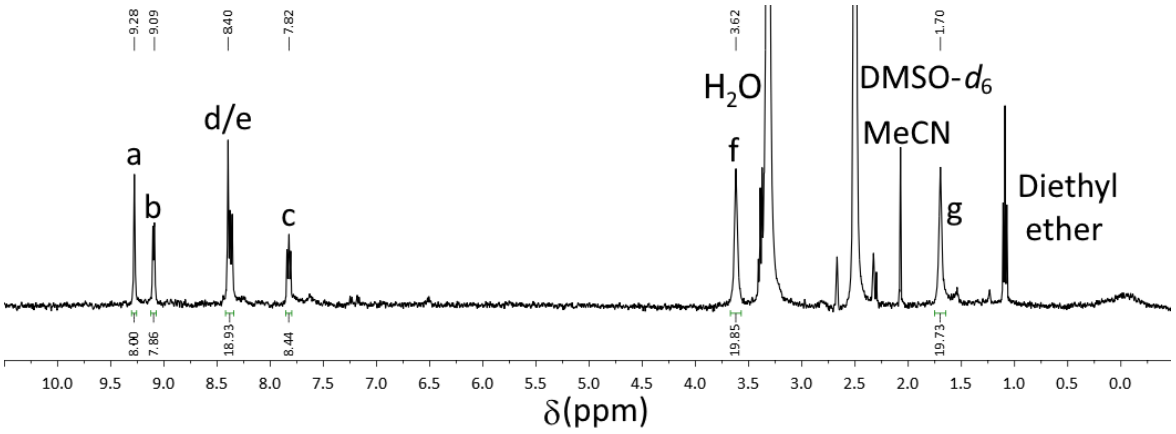

Figure S13: ^{1}H NMR spectrum (400 MHz, DMSO-d_6, 298 K) of $\mathbf{C_{butyl}}$.

2.11 Synthesis of C_{mxy}

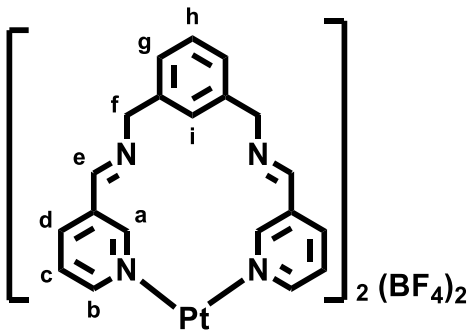

[Pt(3-pyridinecarboxaldehyde)$_4$](BF$_4$)$_2$ (0.095 g, 0.12 mmol, 1.0 eq.) and *m*-xylylenediamine (0.032 mL, 0.24 mmol, 2.0 eq.) were dissolved in MeCN (5 mL) and stirred at RT for 18 h. Diethyl ether (40 mL) was added to the solution and the resulting precipitate collected via centrifugation, washed with DCM once and dried *in vacuo* to afford the product as an off-white solid. Yield: 0.096 g, 0.096 mmol, 80%. ^{1}H NMR (400 MHz, MeCN-d_3) δ: 10.05 (d, J = 1.3 Hz, 4H, H$_a$), 8.95 (d, J = 5.4 Hz, 4H, H$_b$), 8.42 (s, 4H, H$_e$), 8.03 (dt, J = 7.9, 1.6 Hz, 4H, H$_d$), 7.58 (ddd, J = 7.9, 5.8, 0.7 Hz, 4H, H$_c$), 7.43 (s, 2H, H$_i$), 7.39 – 7.34 (m, 2H, H$_h$), 7.24 (d, J = 7.7 Hz, 4H, H$_g$), 4.97 (s, 8H, H$_f$). ^{13}C{^{1}H} NMR (100 MHz, CD$_3$CN) δ: 158.7, 153.1, 150.7, 142.0, 141.3, 136.9, 129.1, 128.6, 126.1, 125.8, 63.1. Pseudo-cryo ESI MS (MeCN) *m/z* = 411.6445 [M – $2BF_4$]$^{2+}$ (calc. for $[C_{40}H_{36}N_8Pt]^{2+}$, 411.6351), 910.2732 [M – BF_4]$^+$ (calc. for $[C_{40}H_{36}N_8PtBF_4]^+$, 910.2746). IR (ATR): ν (cm^{-1}) 3620, 3088, 2886, 1647, 1608, 1485, 1439, 1376, 1317, 1194, 1952, 812, 697, 520.

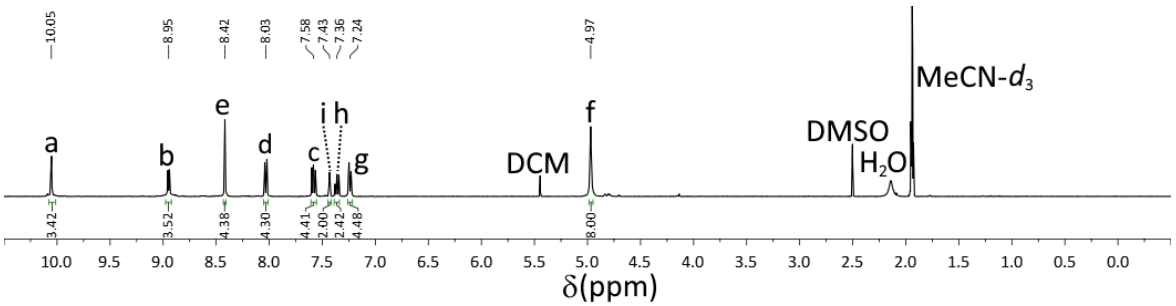

Figure S14: ^{1}H NMR spectrum (400 MHz, MeCN-d_3, 298 K) of $\mathbf{C_{mxy}}$.

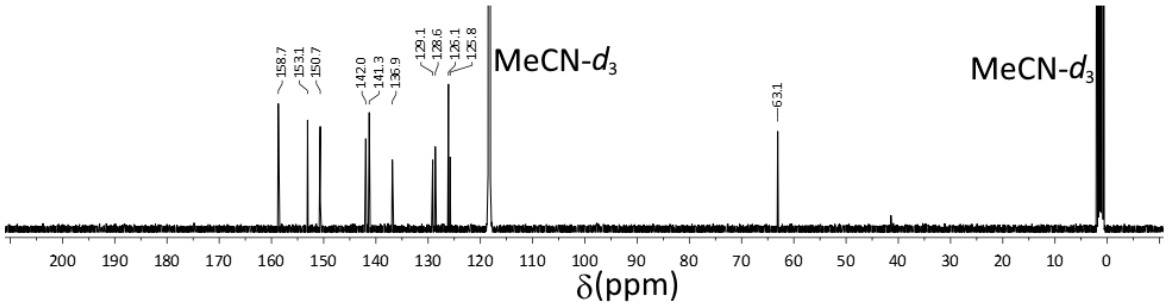

Figure S15: ^{13}C{^{1}H} NMR spectrum (100 MHz, MeCN-d_3, 298 K) of $\mathbf{C_{mxy}}$.

2.12 Synthesis of C_{loop}

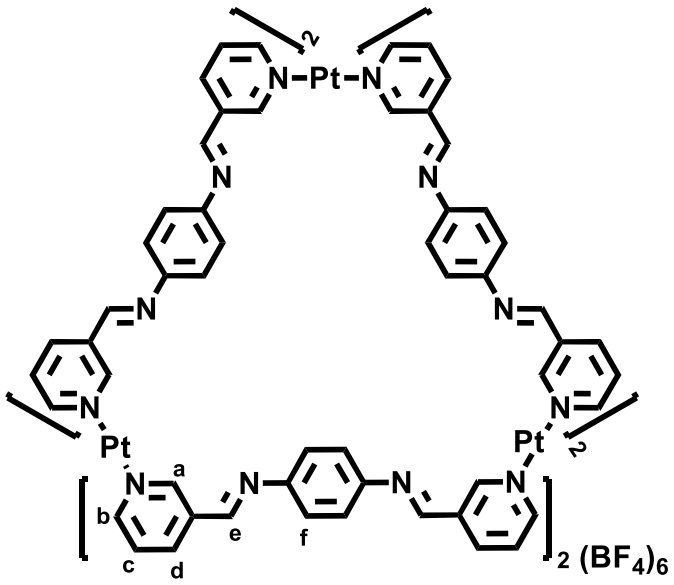

[Pt(3-pyridinecarboxaldehyde)$_4$](BF_4)$_2$ (0.097 g, 0.12 mmol, 3.0 eq.) and *p*-phenylenediamine (0.027 g, 0.27 mmol, 6.0 eq.) were dissolved in MeCN (10 mL) and stirred at 60 °C for 20 h. The reaction mixture was centrifuged and the supernatant discarded. The precipitate was washed with a small volume of MeCN, DCM and ether before drying *in vacuo* to afford the product as a red solid. Yield: 0.060 g, 0.021 mmol, 53%. ^{1}H NMR (400 MHz, DMSO-d_6) δ 10.27 (s, 12H, H_a), 9.39 (d, J = 5.9 Hz, 12H, H_b), 8.77 (s, 12H, H_e), 8.39 (d, J = 8.1 Hz, 12H, H_d), 7.93 – 7.87 (dd,

J = 7.0, 6.3 Hz, 12H, H_c), 7.29 (s, 24H, H_f). $^{13}C\{^1H\}$ NMR (100 MHz, DMSO-d_6) δ: 156.1, 152.8, 150.4, 148.2, 141.7, 135.0, 127.8, 122.6. Pseudo-cryo ESI MS (MeOH) *m/z* = 383.7716 $[M - 6BF_4]^{6+}$ (calc. for $[C_{108}H_{84}N_{24}Pt_3]^{6+}$, 383.7706), 619.1593 $[M - 4BF_4]^{4+}$ (calc. for $[C_{108}H_{84}N_{24}Pt_3B_2F_8]^{4+}$, 619.1581). Anal. calc. for $C_{108}H_{84}N_{24}Pt_3B_6F_{24}•2CH_2Cl_2$: C, 43.79%; H, 3.08%; N, 10.94%. Found: C, 43.84%; H, 3.19%; N, 11.33%. IR (ATR): v (cm^{-1}) 3616, 3376, 3086, 1702, 1627, 1580, 1508, 1496, 1438, 1051, 840, 814, 695, 520.

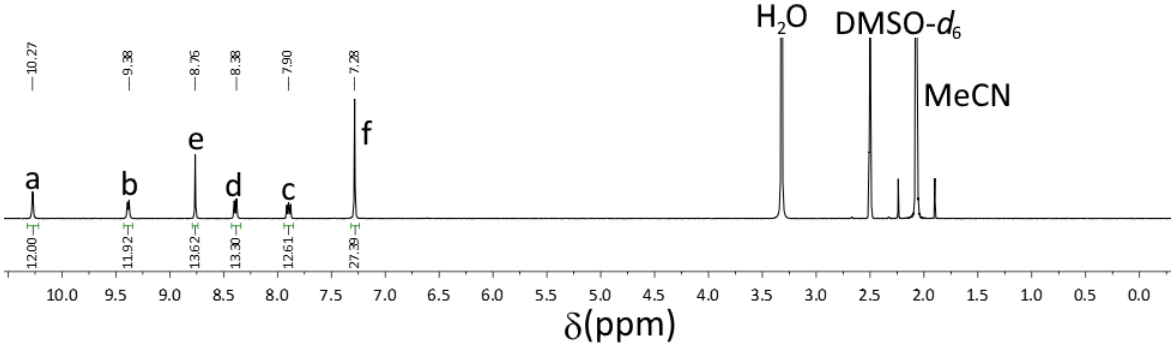

Figure S16: ^1H NMR spectrum (400 MHz, DMSO-d_6, 298 K) of $\mathbf{C_{loop}}$.

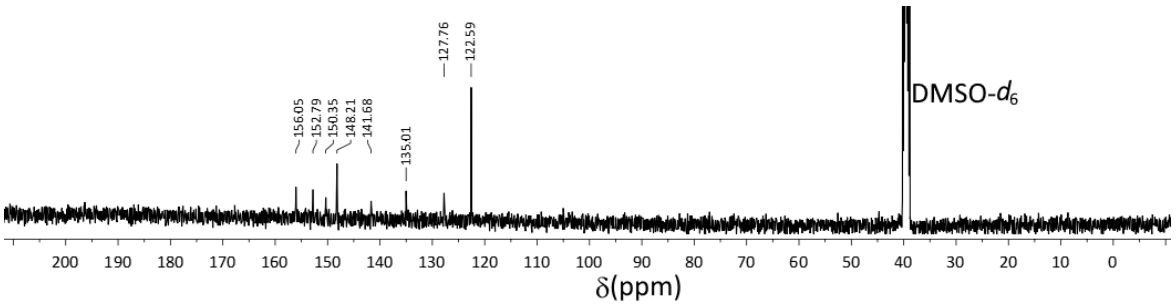

Figure S17: $^{13}C\{^1H\}$ NMR spectrum (100 MHz, DMSO-d_6, 298 K) of $\mathbf{C_{loop}}$.

2.13 Synthesis of C_{hydra}

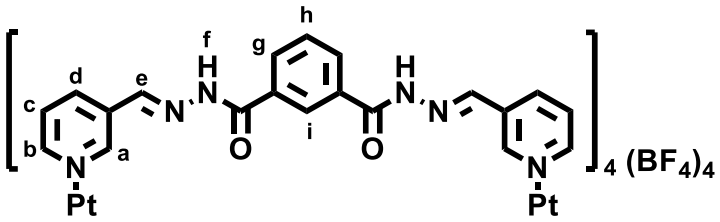

[Pt(3-pyridinecarboxaldehyde)$_4$](BF_4)$_2$ (0.0820 g, 0.103 mmol, 2.0 eq.) and 1,3-dihydrazide-1,3-benzenedicarboxylic acid (0.0398 g, 0.205 mmol, 4.0 eq.) were dissolved in DMSO (3 mL) and stirred at RT for 18 h. Ethyl acetate (30 mL) was added to the solution and the resulting precipitate collected via centrifugation, washed with EtOAc, MeOH, and DCM, and dried *in vacuo* to afford the product as an off-white solid. Yield: 0.103 g, 0.046 mmol, 89%. ^{1}H NMR (500 MHz, DMSO-d_6) δ: 12.51 (s, 8H, H_f), 9.70 (s, 8H, H_a), 9.33 (d, J = 5.9 Hz, 8H, H_b), 8.71 (s, 4H, H_i), 8.57 (s, 8H, H_e), 8.38 (d, J = 8.0 Hz, 8H, H_d), 8.25 (d, J = 8.1 Hz, 8H, H_g), 7.89 – 7.84 (m, 8H, H_c), 7.74 (t, J = 7.7 Hz, 4H, H_h). ^{13}C{^{1}H} NMR (125 MHz, DMSO-d_6): δ 162.0, 152.1, 149.7, 143.3, 143.2, 138.7, 134.1, 132.6, 131.5, 128.0, 127.1. HR ESI MS (DMSO) m/z = 469.8698 [M – 4BF_4]$^{4+}$ (calc. for [$C_{80}H_{64}N_{24}O_8Pt_2$]$^{4+}$, 469.6153), 655.1603 [M – 3BF_4]$^{3+}$ (calc. for [$C_{80}H_{64}N_{24}O_8Pt_2BF_4$]$^{3+}$, 655.1549), 1026.2427 [M-2BF_4]$^{2+}$ (calc. for [$C_{80}H_{64}N_{24}O_8Pt_2B_2F_8$]$^{2+}$, 1026.2341). IR (ATR): ν (cm^{-1}) 3589, 3411, 3250, 3078, 1664, 1544, 1482, 1432, 1362, 1326, 1295, 1057, 816, 695, 520.

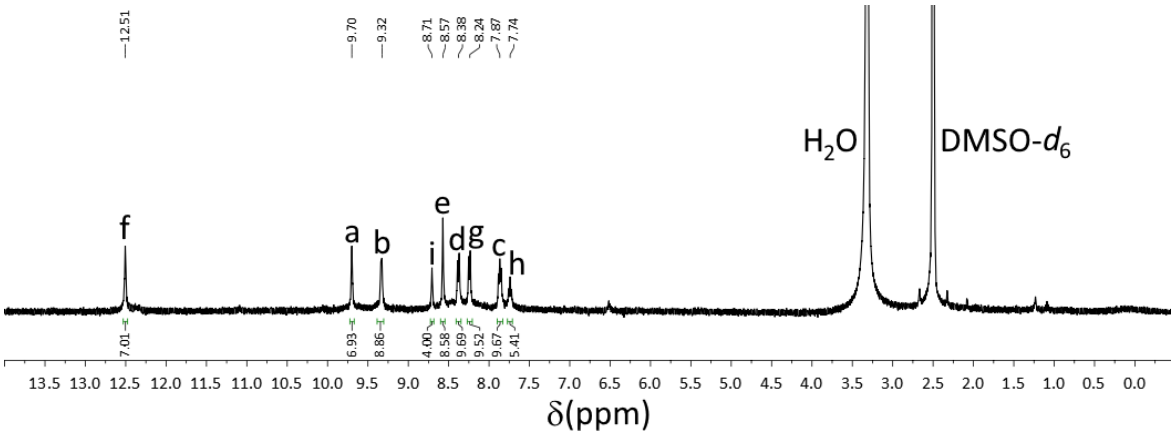

Figure S18: ^{1}H NMR spectrum (400 MHz, DMSO-d_6, 298 K) of $\mathbf{C_{hydra}}$.

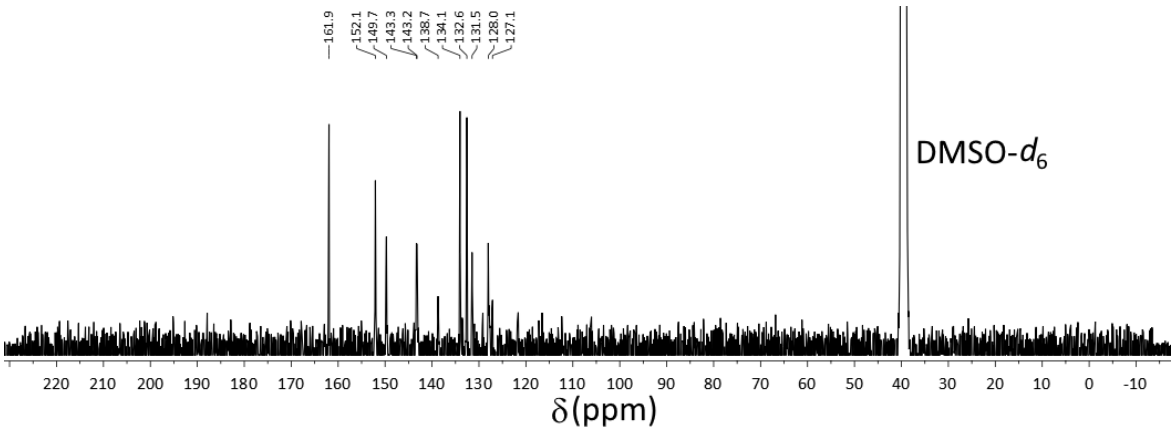

Figure S19: $^{13}C\{^{1}H\}$ NMR spectrum (125 MHz, DMSO-d_6, 298 K) of $\mathbf{C_{hydra}}$.

3 ESI mass spectra

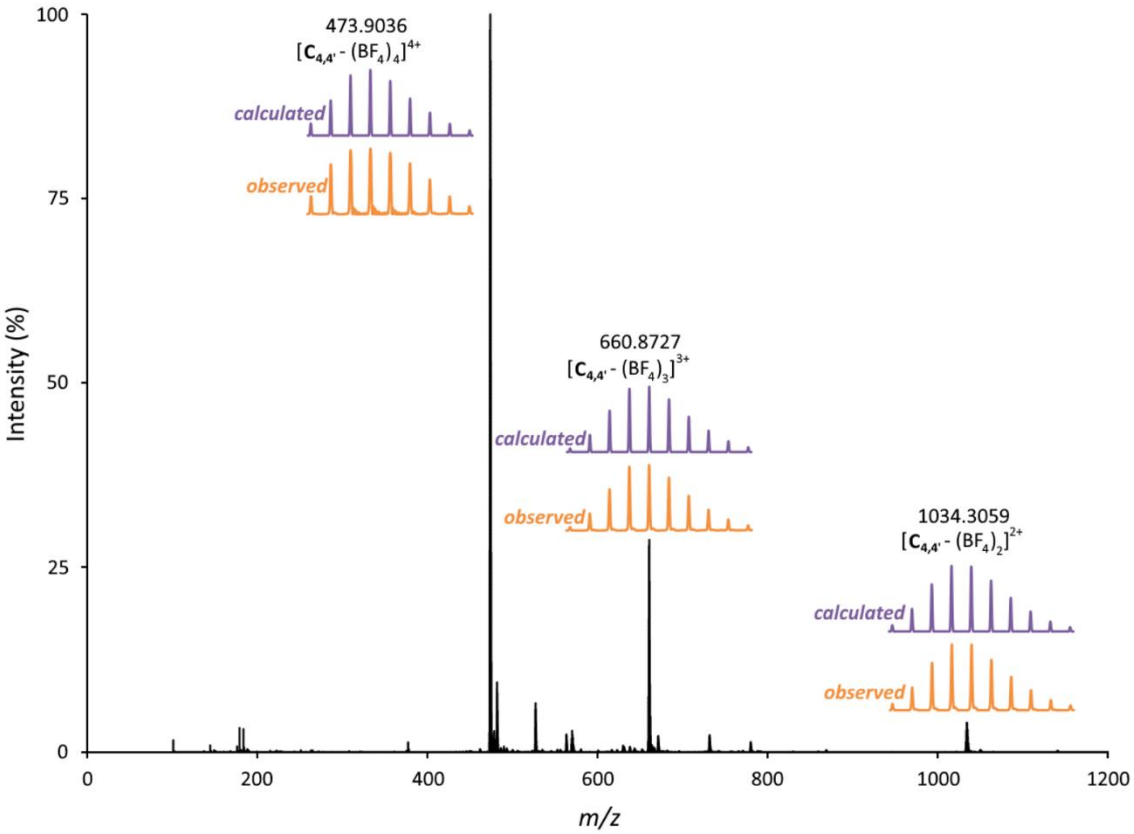

Figure S20: HR ESI mass spectrum (MeCN) of $\mathbf{C_{4,4'}}$ and its isotopic patterns.

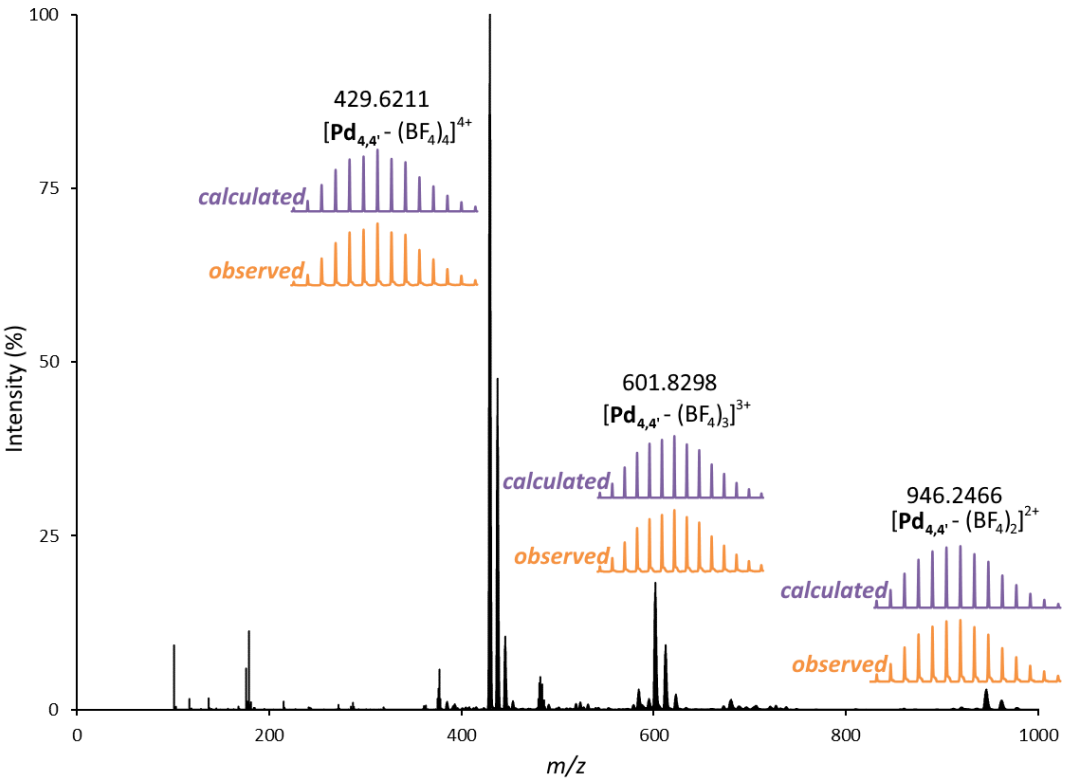

Figure S21: HR ESI mass spectrum (MeOH) of **$Pd_{4,4'}$** and its isotopic patterns.

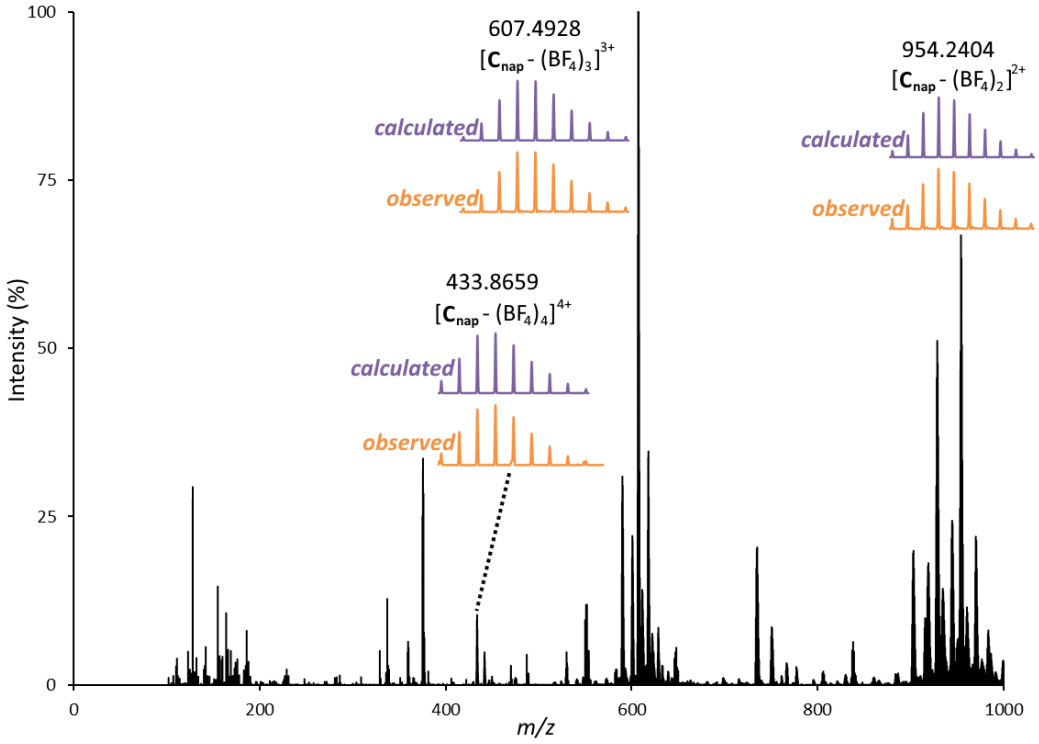

Figure S22: HR ESI mass spectrum (MeCN) of **C_{nap}** and its isotopic patterns.

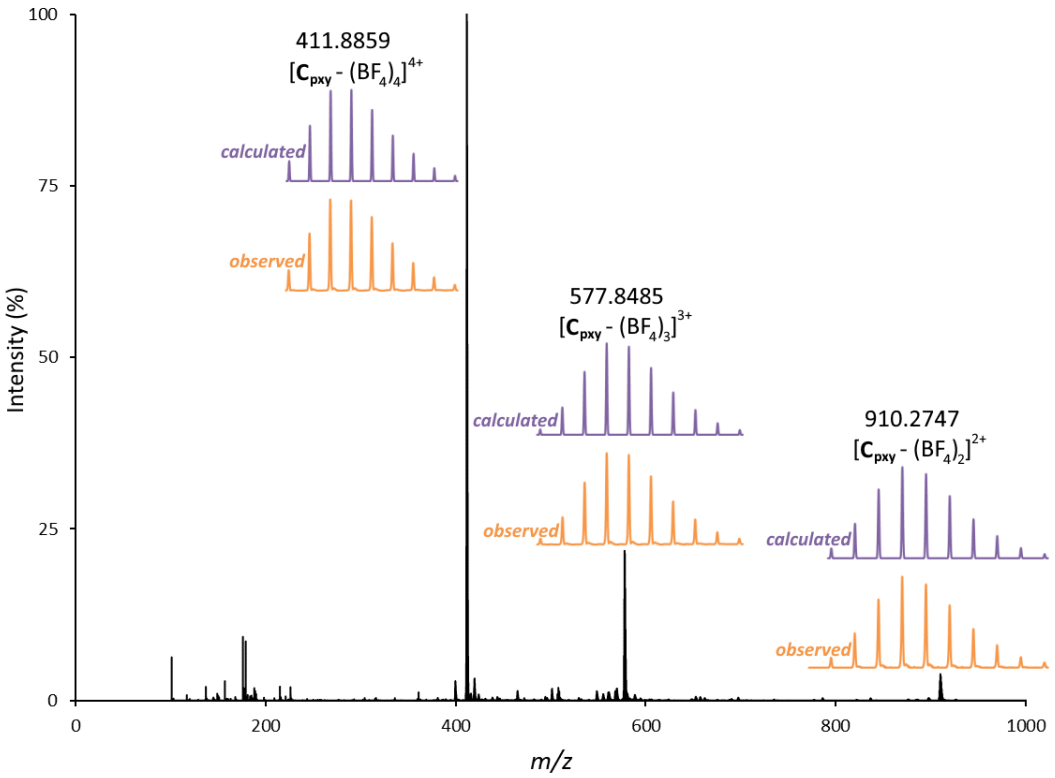

Figure S23: Pseudo-cryo ESI mass spectrum (MeCN) of $\mathbf{C_{pxy}}$ and its isotopic patterns.

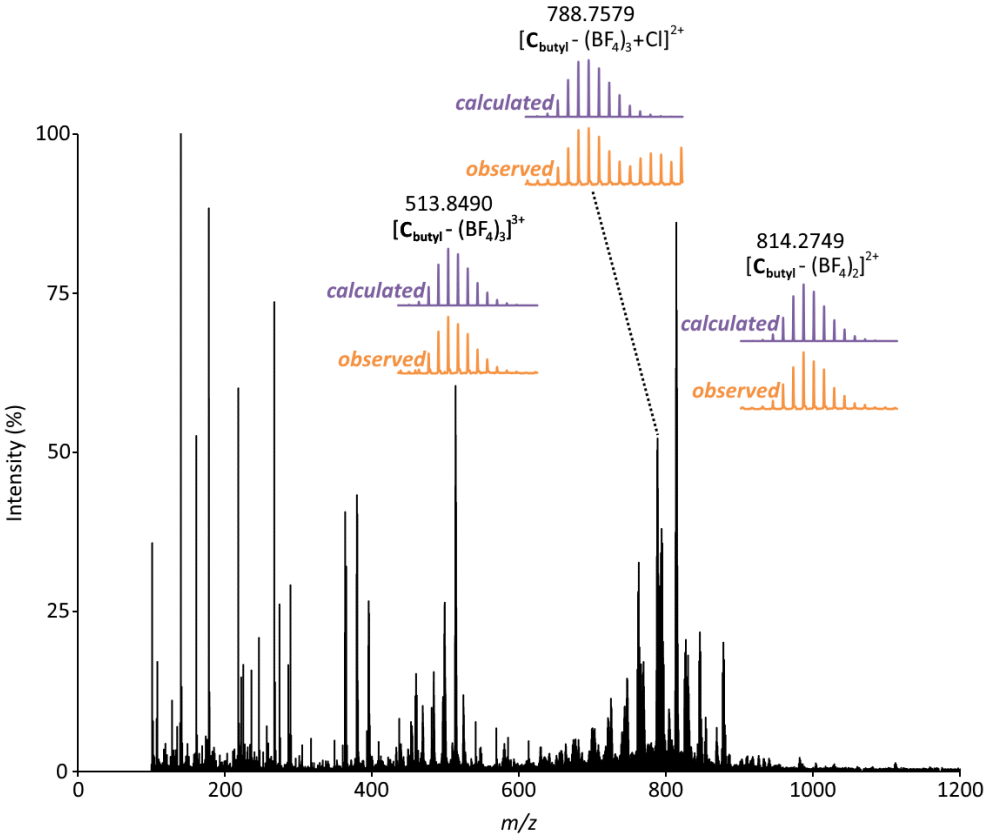

Figure S24: HR ESI mass spectrum (MeCN) of $\mathbf{C_{butyl}}$ and its isotopic patterns.

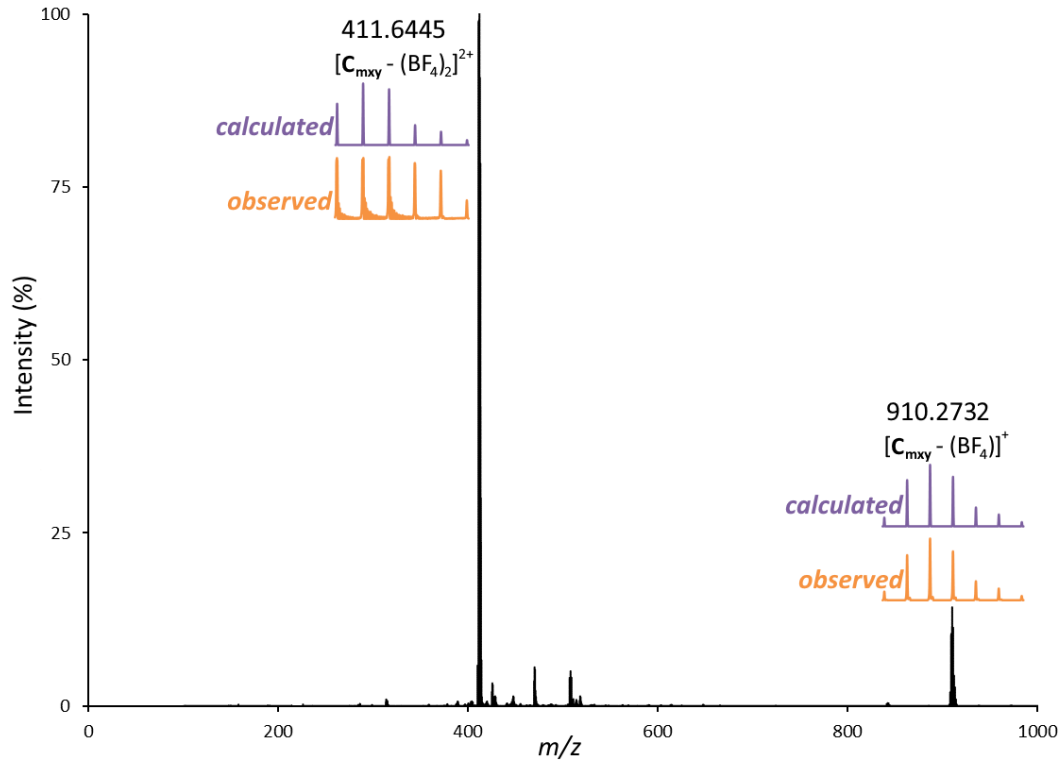

Figure S25: Pseudo-cryo mass spectrum (MeCN) of $\mathbf{C_{mxy}}$ and its isotopic patterns.

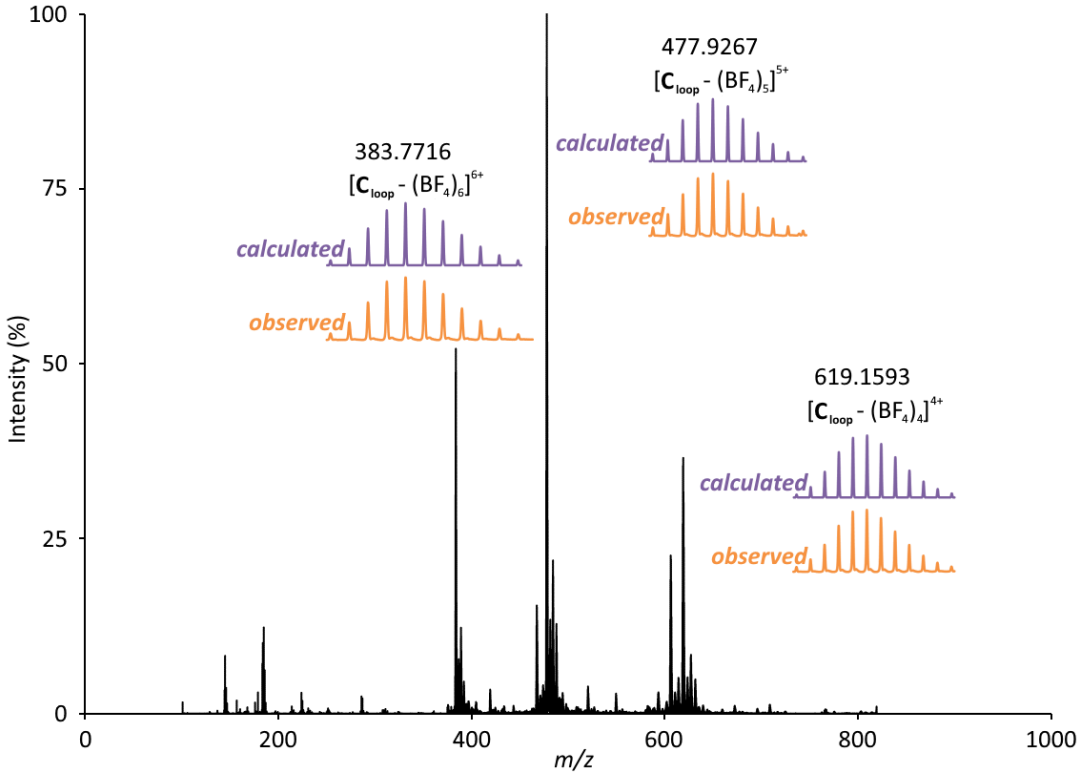

Figure S26: Pseudo-cryo ESI mass spectrum (MeOH) of $\mathbf{C_{loop}}$ and its isotopic patterns.

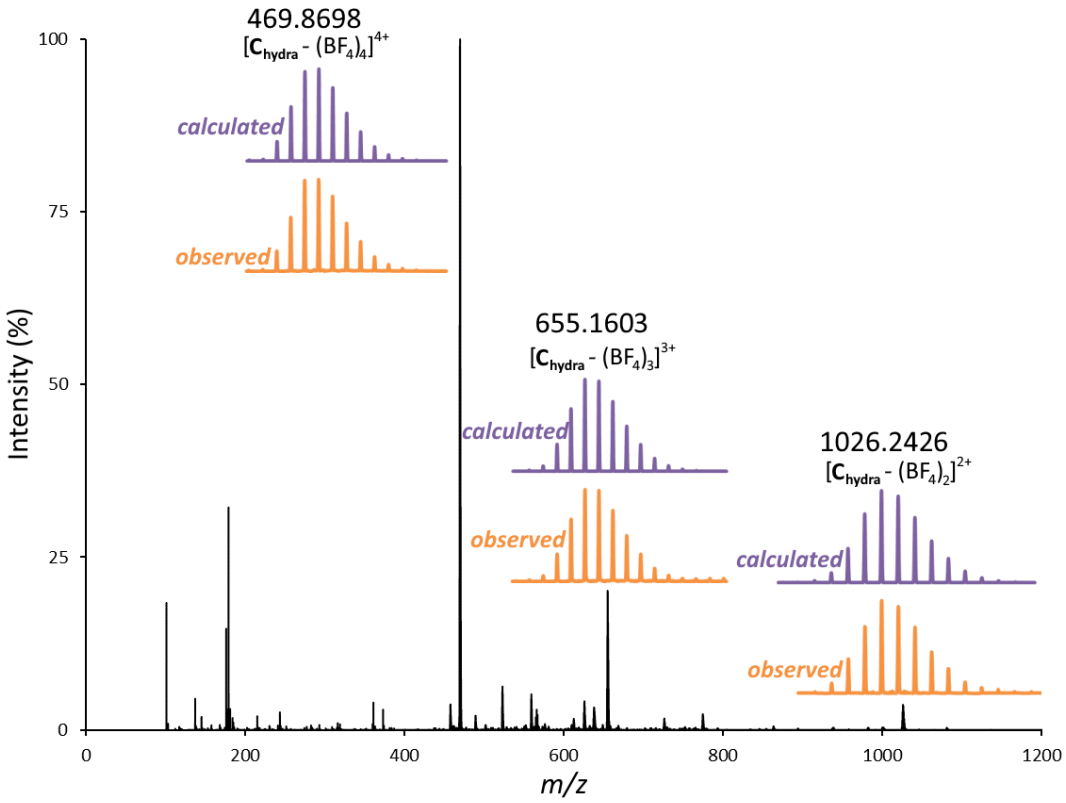

Figure S27: HR ESI mass spectrum of $\mathbf{C_{hydra}}$ and its isotopic patterns.

4 ^{1}H DOSY NMR data

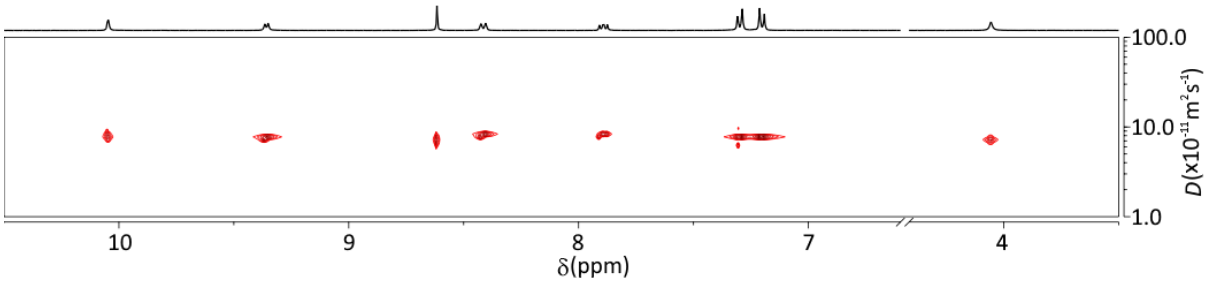

Figure S28: Partial ^{1}H NMR and DOSY spectra (400 MHz, DMSO-d_6, 298 K) for $\mathbf{C_{4,4'}}$.

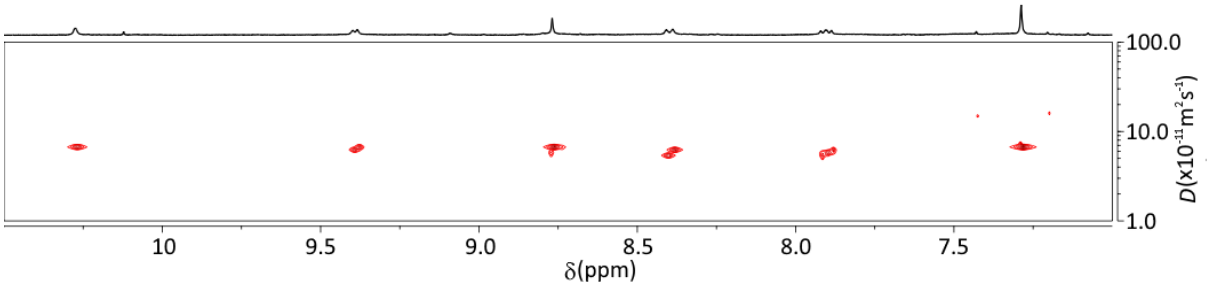

Figure S29: Partial ^{1}H NMR and DOSY spectra (400 MHz, DMSO-d_6, 298 K) for $\mathbf{C_{loop}}$.

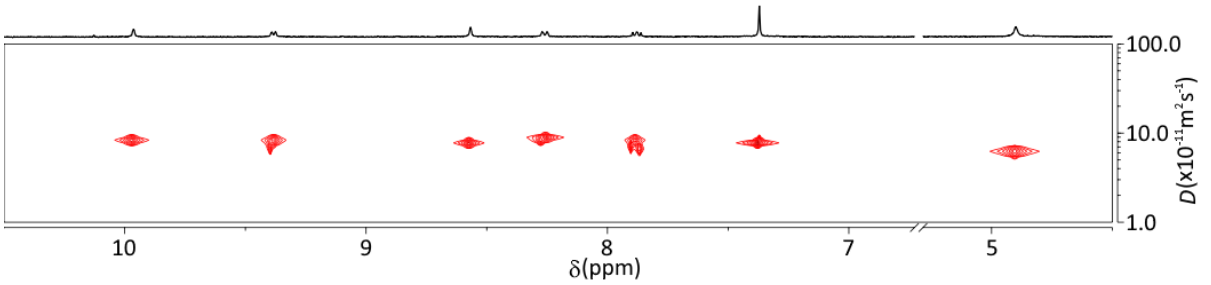

Figure S30: Partial ^{1}H NMR and DOSY spectra (400 MHz, DMSO-d_6, 298 K) for $\mathbf{C_{pxy}}$.

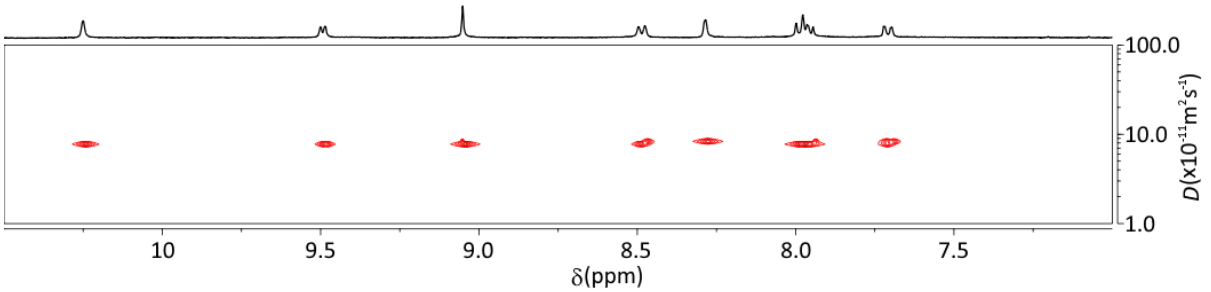

Figure S31: Partial ^{1}H NMR and DOSY spectra (400 MHz, DMSO-d_6, 298 K) for $\mathbf{C_{nap}}$.

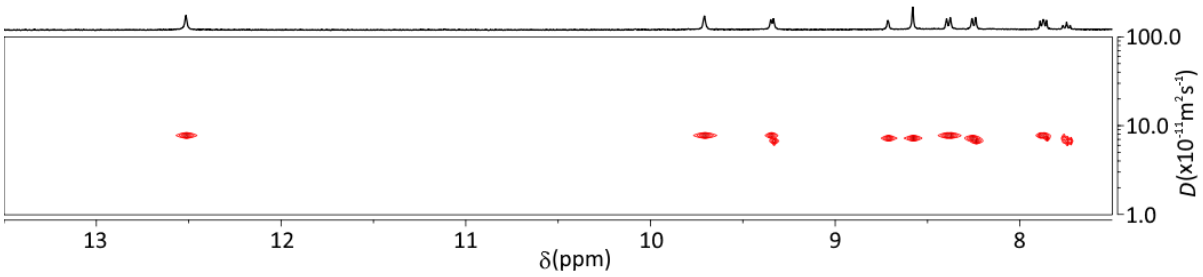

Figure S32: Partial ^{1}H NMR and DOSY spectra (400 MHz, DMSO-d_6, 298 K) for $\mathbf{C_{hydra}}$.

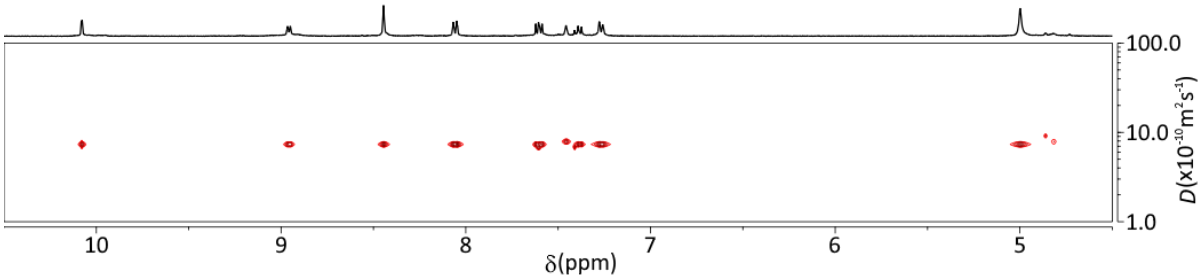

Figure S33: Partial ^{1}H NMR and DOSY spectra (400 MHz, MeCN-d_3, 298 K) for $\mathbf{C_{mxy}}$.

Table S1: Diffusion coefficients of relevant compounds (400 MHz, DMSO-d_6, 298 K).

Compound	Molecular Weight (g mol^{-1})	Diffusion Coefficient (x10^{-10} m^2 s^{-1})
4,4′-diaminodiphenylmethane	198.27	2.19
$\mathbf{C_{4,4'}}$	2243.23	0.79
p -phenylenediamine	108.14	4.74
$\mathbf{C_{loop}}$	2824.10	0.62
p-xylylenediamine	136.20	2.76
$\mathbf{C_{pxy}}$	1994.95	0.78
2,7-diaminonapthalene	158.20	3.11
$\mathbf{C_{nap}}$	2082.97	0.80
Isophthalic dihydrazide	194.19	2.87
$\mathbf{C_{hydra}}$	2226.93	0.73
m-xylylenediamine[a]	136.20	20.06
$\mathbf{C_{mxy}}$[a]	997.48	7.35

[a] Diffusion coefficient is given for M-xylylenediamine and $\mathbf{C_{mxy}}$ in MeCN-d_6 due to insolubility of the complex in DMSO-d_6.

5 UV-Vis absorption spectra

UV-Vis absorption spectra of the Pt(II) architectures were obtained on 1 x 10^{-5} mol L^{-1} solutions (DMSO or MeCN) using a quartz cuvette.

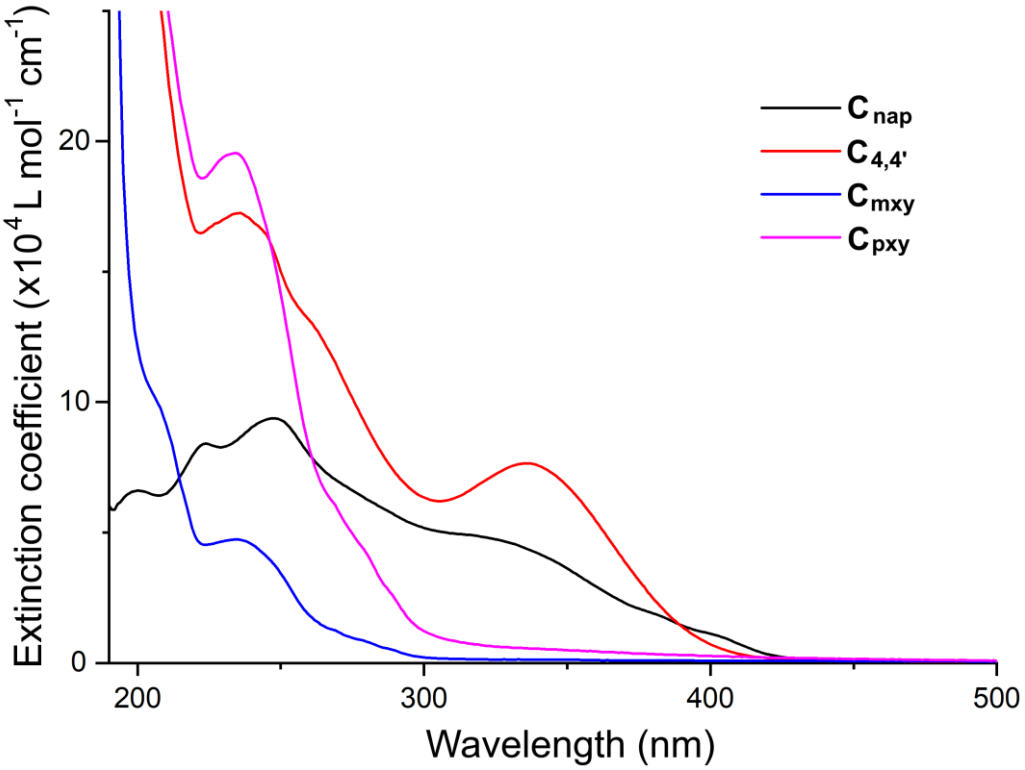

Figure S34: UV-vis spectra of Pt(II) architectures that are soluble in MeCN.

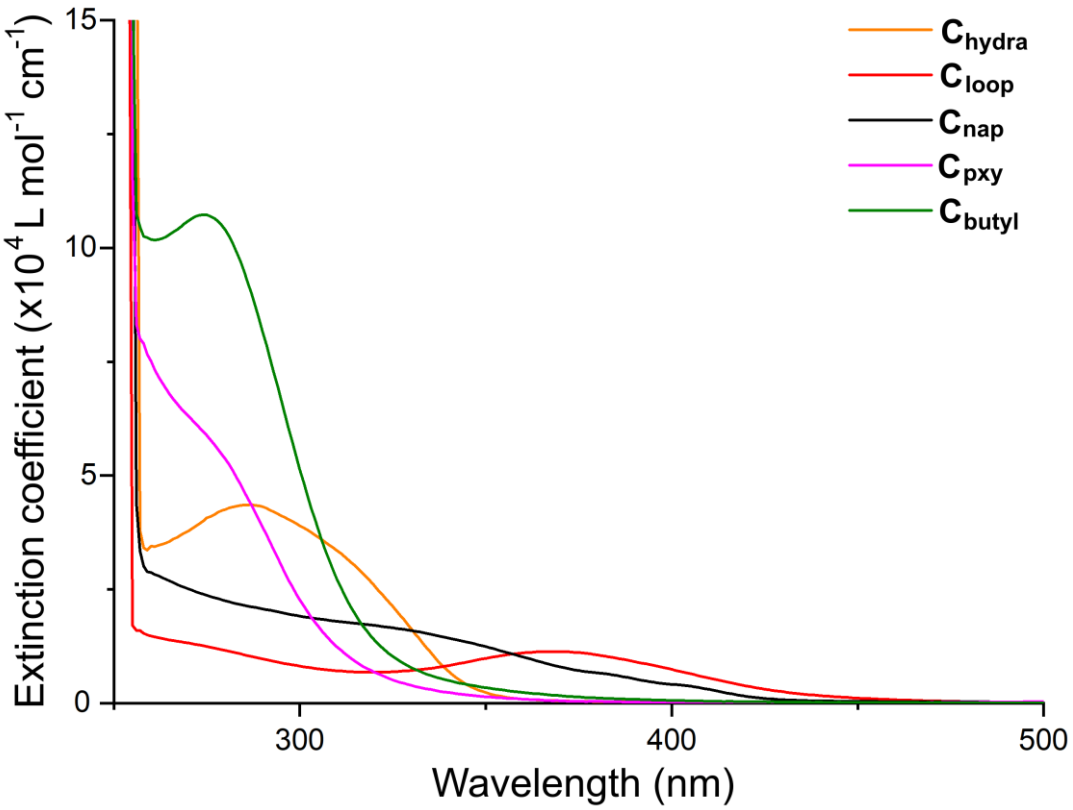

Figure S35: UV-vis spectra of Pt(II) architectures that are soluble in DMSO.

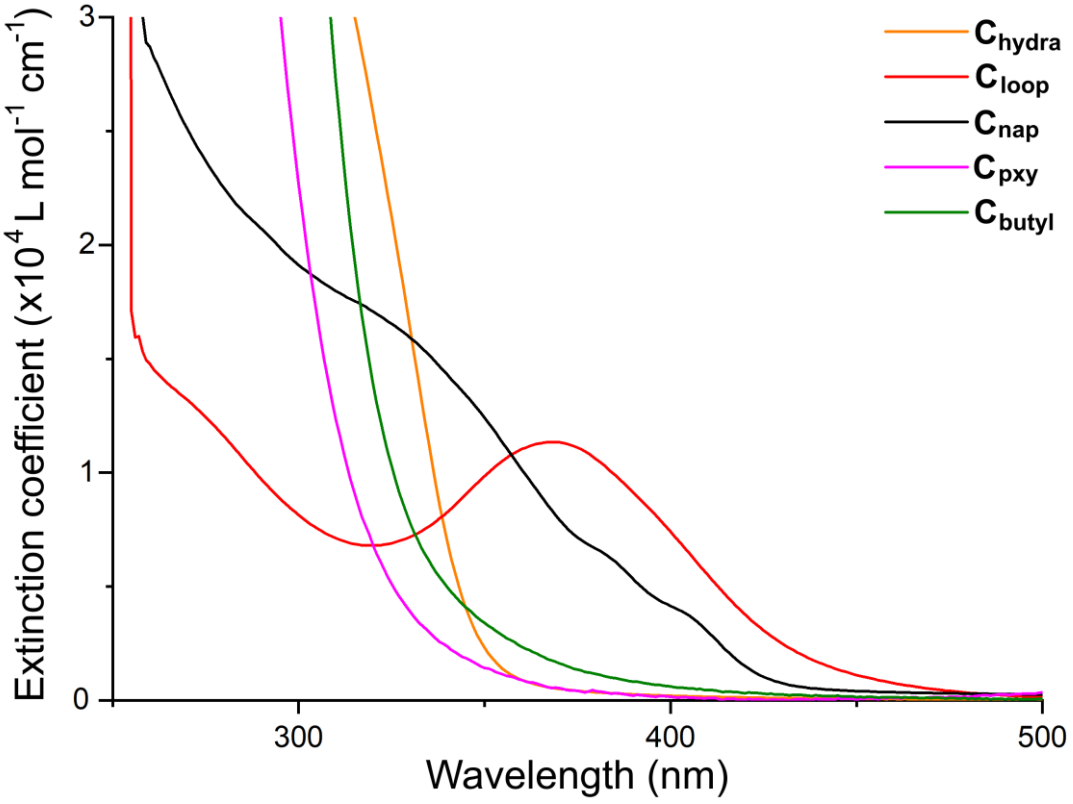

Figure S36: UV-vis spectra of Pt(II) architectures that are soluble in DMSO (expanded region at low extinction coefficient).

6 ^{1}H NMR studies

6.1 ^{1}H NMR synthesis studies

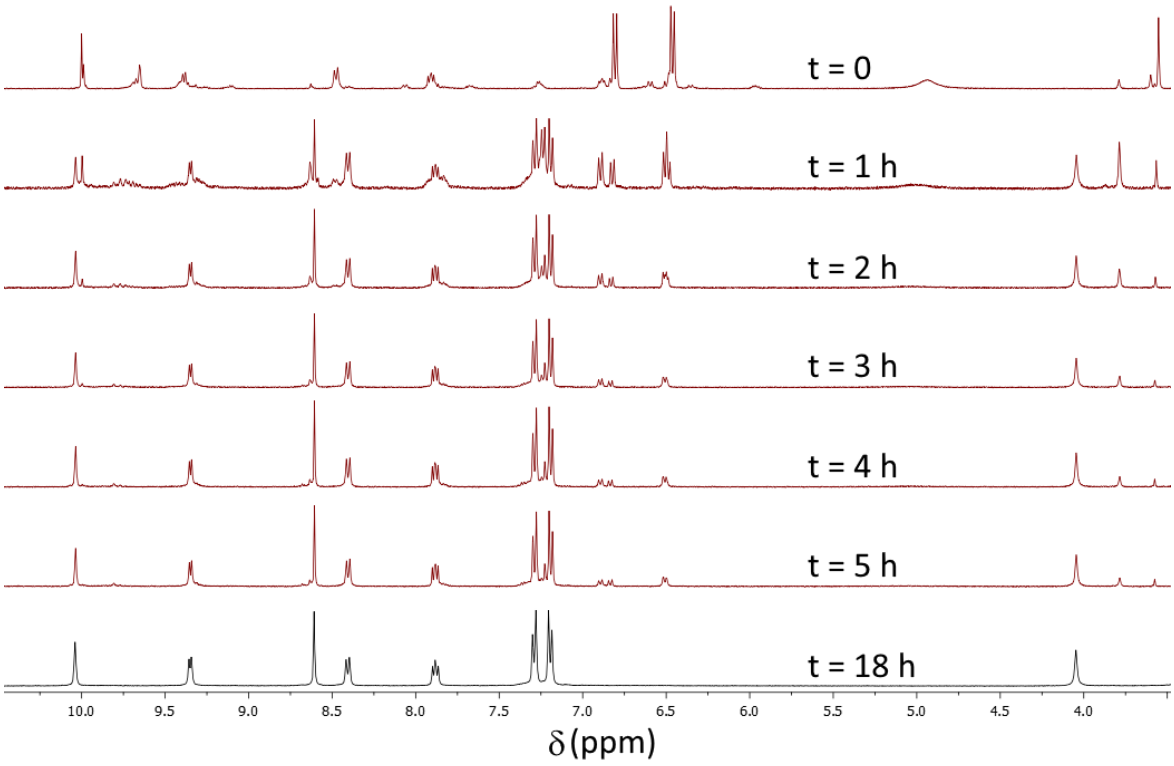

Figure S37: Partial stacked ^{1}H NMR spectra (400 MHz, 298 K, DMSO-d_6) spectra for the reaction of [Pt(**3-py**)$_4$](BF$_4$)$_4$ with 4,4′-diaminodiphenylmethane to produce **C$_{4,4'}$** over 18 h.

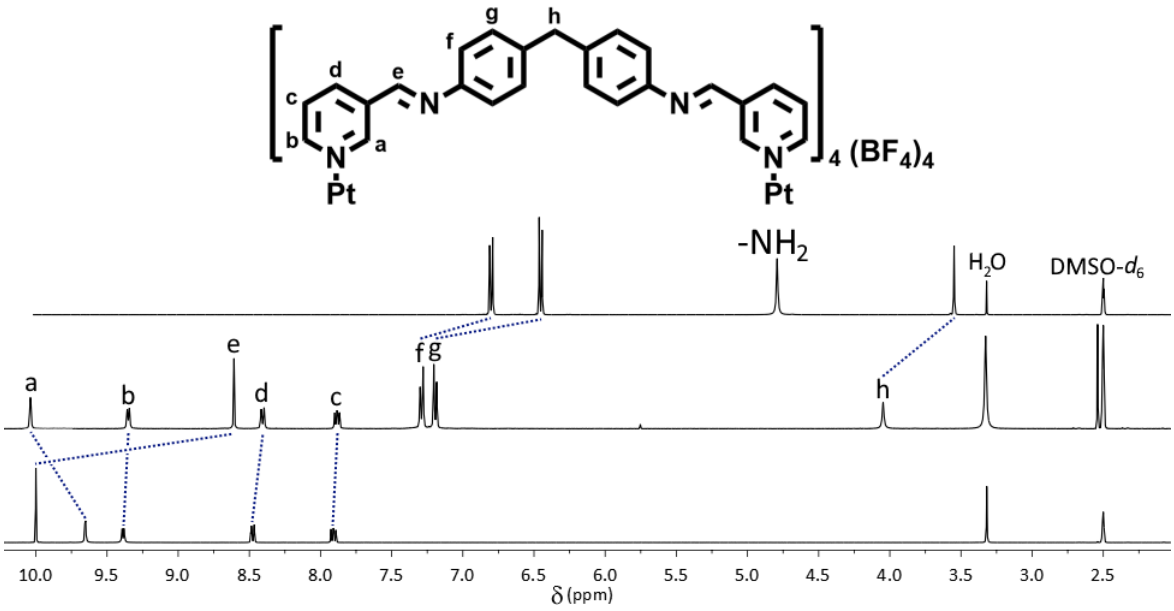

Figure S38: Partial stacked ^{1}H NMR spectra (400 MHz, 298 K, DMSO-d_6) showing proton environments for 4,4′-diaminodiphenylmethane (top), **C$_{4,4'}$** (middle) and [Pt(**3-py**)$_4$](BF$_4$)$_2$ (bottom).

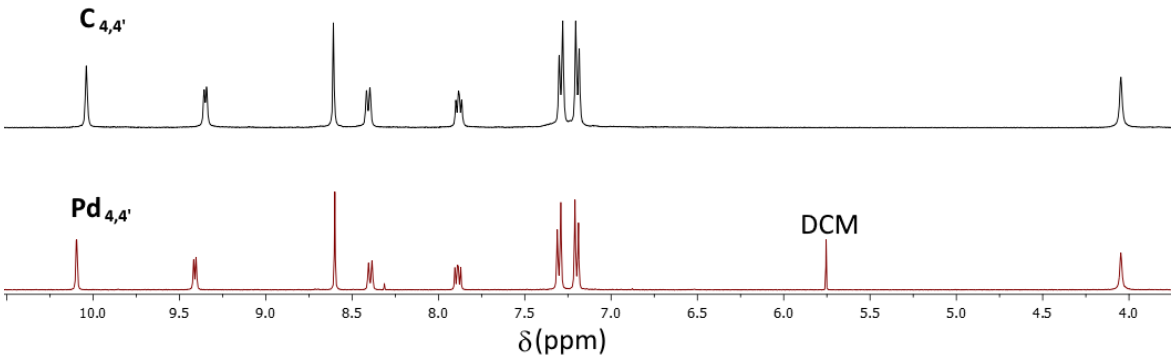

Figure S39: Partial stacked ^{1}H NMR spectra (400 MHz, DMSO-d_6, 298 K) comparing the spectra for $\mathbf{C_{4,4'}}$ and Chand and co-workers analogous palladium cage ($\mathbf{Pd_{4,4'}}$).[8]

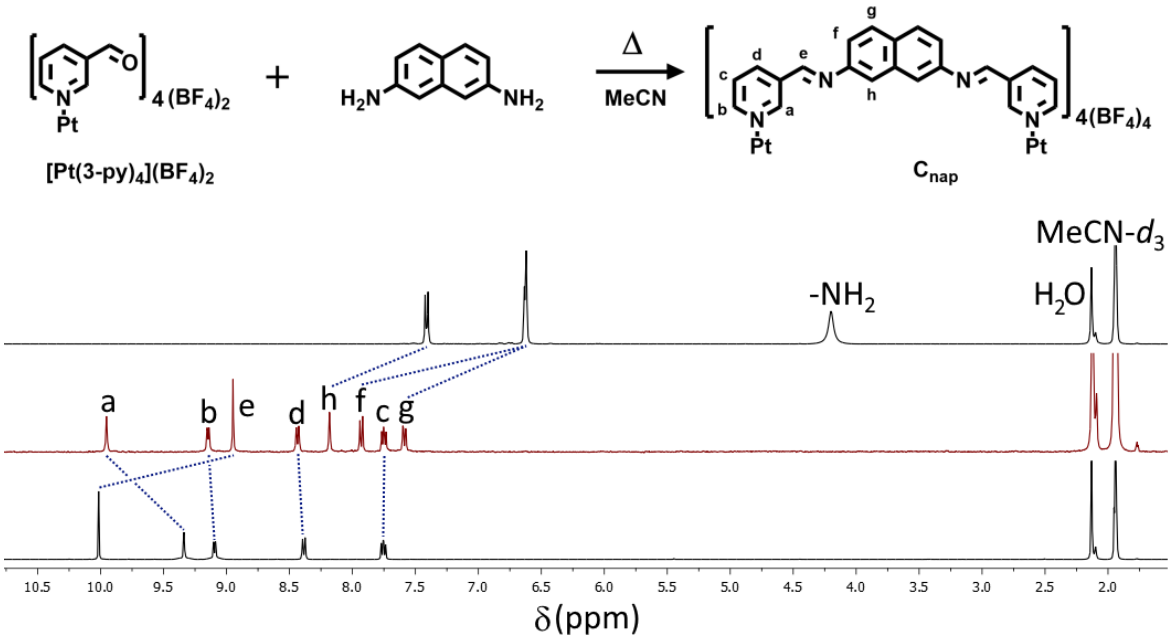

Figure S40: Approach to the synthesis of $\mathbf{C_{nap}}$ combining [Pt(**3-py**)$_4$](BF$_4$)$_2$ (2 eq.) with 2,7-diaminonapthalene (4 eq.) and partial stacked ^{1}H NMR spectra (400 MHz, 298 K, MeCN-d_3) showing the formation of $\mathbf{C_{nap}}$ from its constituents, 2,7-diaminonapthalene (top), $\mathbf{C_{nap}}$ (middle) and [Pt(**3-py**)$_4$](BF$_4$)$_2$ (bottom).

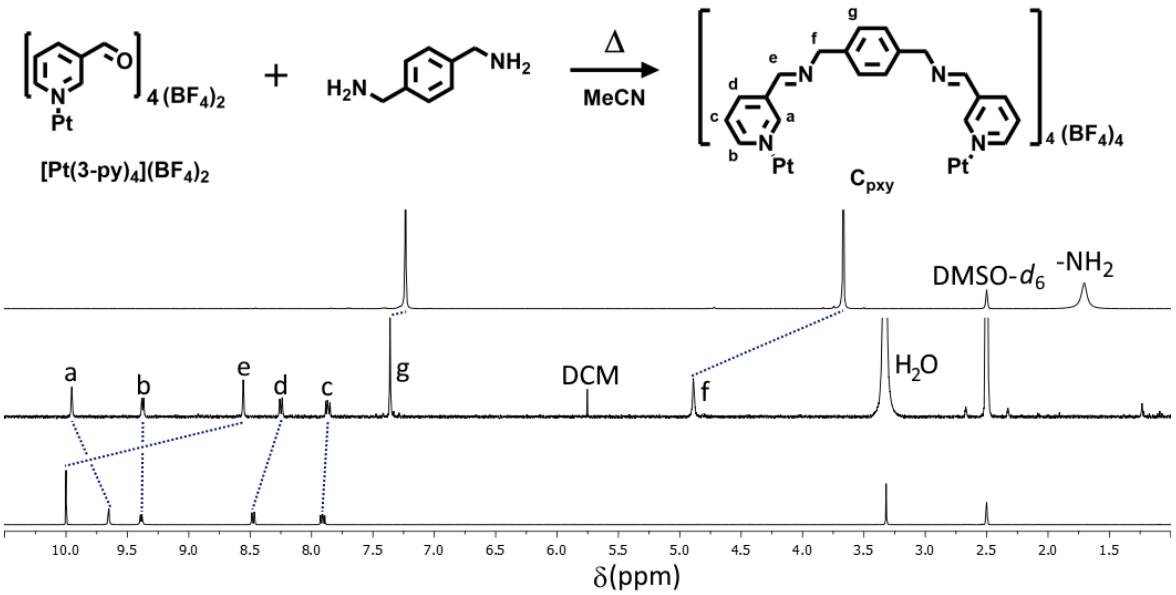

Figure S41: Approach to the synthesis of $\mathbf{C_{pxy}}$ combining [Pt(**3-py**)$_4$](BF$_4$)$_2$ (2 eq.) and *p*-xylylenediamine (4 eq.) and partial stacked ^{1}H NMR spectra (400 MHz, 298 K, DMSO-d_6) showing the formation of $\mathbf{C_{pxy}}$ from its constituents, *p*-xylylenediamine (top), $\mathbf{C_{pxy}}$ (middle) and [Pt(**3-py**)$_4$](BF$_4$)$_2$ (bottom).

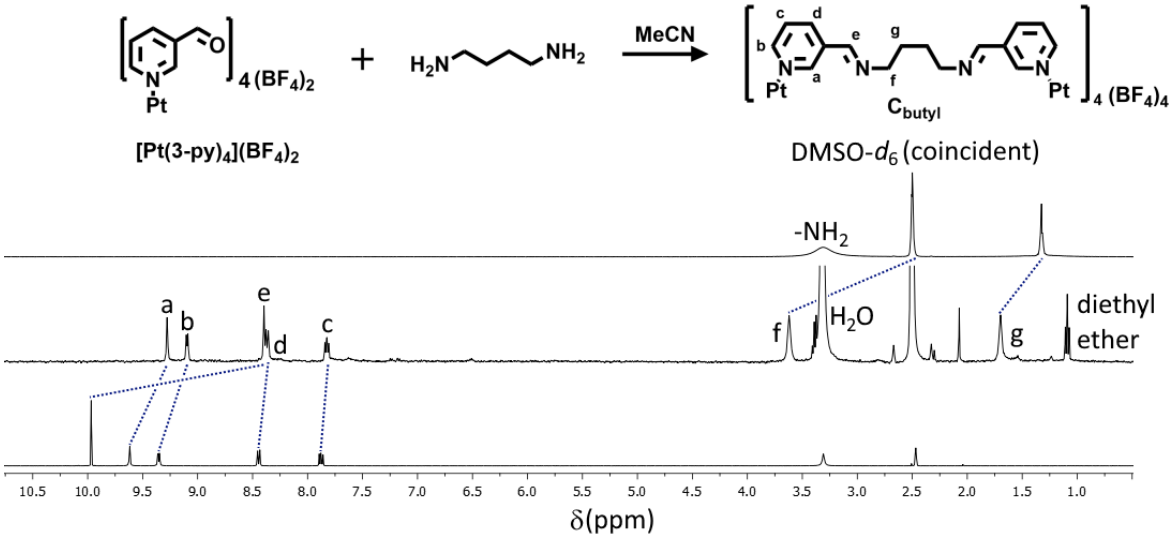

Figure S42: Approach to the synthesis of $\mathbf{C_{butyl}}$ combining [Pt(**3-py**)$_4$](BF$_4$)$_2$ (2 eq.) and 1,4-butadiamine (4 eq.) and partial stacked ^{1}H NMR spectra (400 MHz, 298 K, DMSO-d_6) showing the formation of $\mathbf{C_{butyl}}$ from its constituents, 1,4-butadiamine (top), $\mathbf{C_{butyl}}$ (middle) and [Pt(**3-py**)$_4$](BF$_4$)$_2$ (bottom).

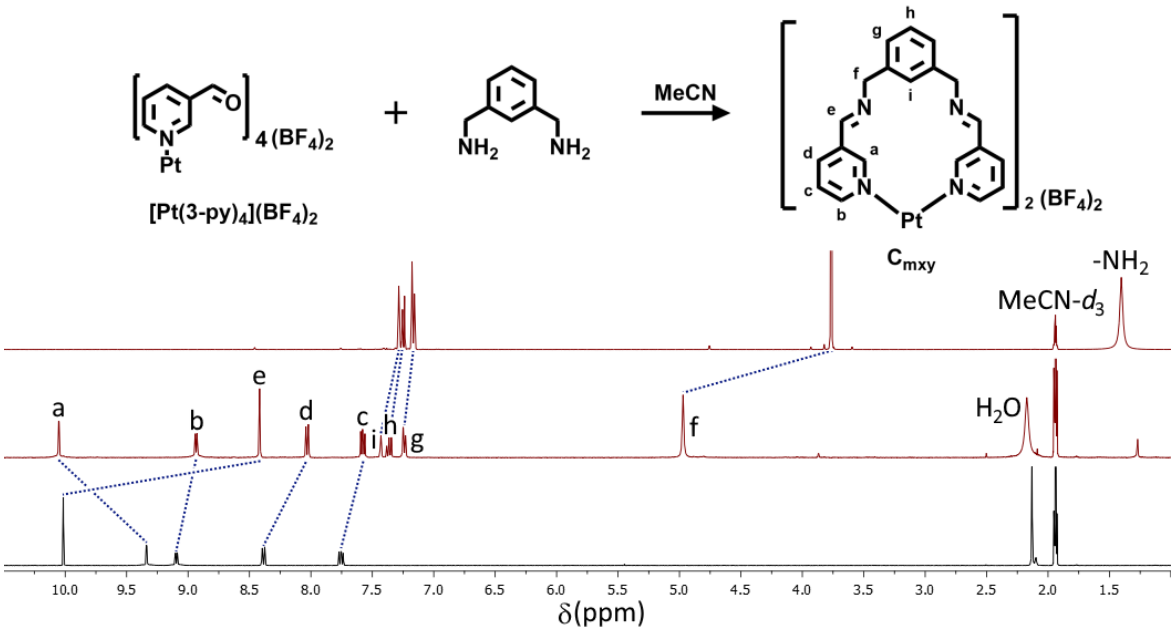

Figure S43: Approach to the synthesis of $\mathbf{C_{mxy}}$ combining [Pt(**3-py**)$_4$](BF$_4$)$_2$ (1 eq.) and *m*-xylylenediamine (2 eq.) and partial stacked ^{1}H NMR spectra (400 MHz, 298 K, MeCN-d_3) showing the formation of $\mathbf{C_{mxy}}$ from its constituents, *m*-xylylenediamine (top), $\mathbf{C_{mxy}}$ (middle) and [Pt(**3-py**)$_4$](BF$_4$)$_2$ (bottom).

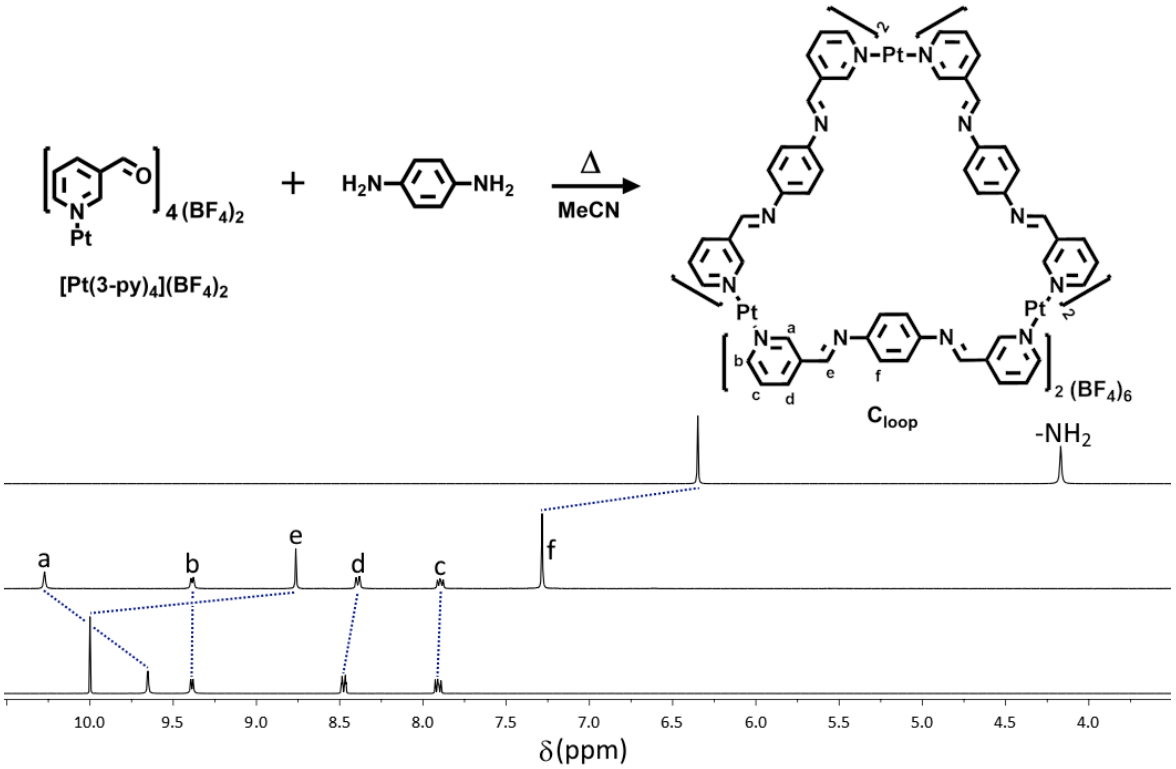

Figure S44: Approach to the synthesis of $\mathbf{C_{loop}}$ combining [Pt(**3-py**)$_4$](BF$_4$)$_2$ (3 eq.) and *p*-phenylenediamine (6 eq.) and partial stacked ^{1}H NMR spectra (400 MHz, 298 K, DMSO-d_6) showing the formation of $\mathbf{C_{loop}}$ from its constituents, *p*-phenylenediamine (top), $\mathbf{C_{loop}}$ (middle) and [Pt(**3-py**)$_4$](BF$_4$)$_2$ (bottom).

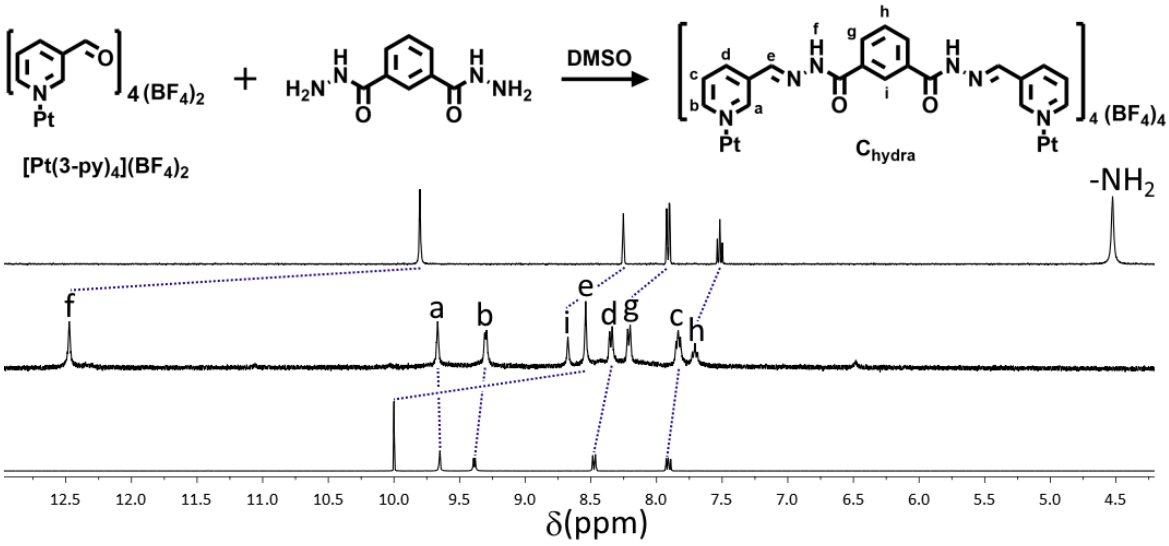

Figure S45: Approach to the synthesis of $\mathbf{C_{hydra}}$ combining [Pt(**3-py**)$_4$](BF$_4$)$_2$ (2 eq.) and isophthalic dihydrazide (4 eq.) and partial stacked ^{1}H NMR spectra (400 MHz, 298 K, DMSO-d_6) showing the formation of $\mathbf{C_{hydra}}$ from its constituents, isophthalic dihydrazide (top), $\mathbf{C_{hydra}}$ (middle) and [Pt(**3-py**)$_4$](BF$_4$)$_2$ (bottom).

6.2 $\mathbf{C_{pxy}}$ ^{1}H NMR scale synthesis via the symmetry interaction approach

To determine if we were able to synthesise the diimine architectures using the symmetry interaction approach, we attempted to prepare one of the cages from the preformed diamine ligand. $\mathbf{C_{pxy}}$ was chosen as it is the smallest [Pt$_2$L$_4$]$^{4+}$ cage formed that has rigidity within the backbone of the ligand. While a synthetic procedure has been reported for the ligand $\mathbf{L_{pxy}}$, we used a more standard method to acquire the compound.[3-4] We combined $\mathbf{L_{pxy}}$ with [Pt(DMSO)$_2$(Cl)$_2$] and AgBF$_4$ in MeCN-d_3 or DMSO-d_6 and stirred it at RT/heated at 60 °C for 3 days while monitoring via ^{1}H NMR spectroscopy. Out of all the reaction mixtures, only heating in MeCN-d_3 at 60 °C after 24 h showed any formation of $\mathbf{C_{pxy}}$ (Figure S46). However, it was formed only in a minor amount. Heating the reaction mixture for longer however did not bring about an increase in the amount of cage formed, but rather the decomposition of the ligand to the corresponding starting materials **3-py** and *p*-xylylenediamine.

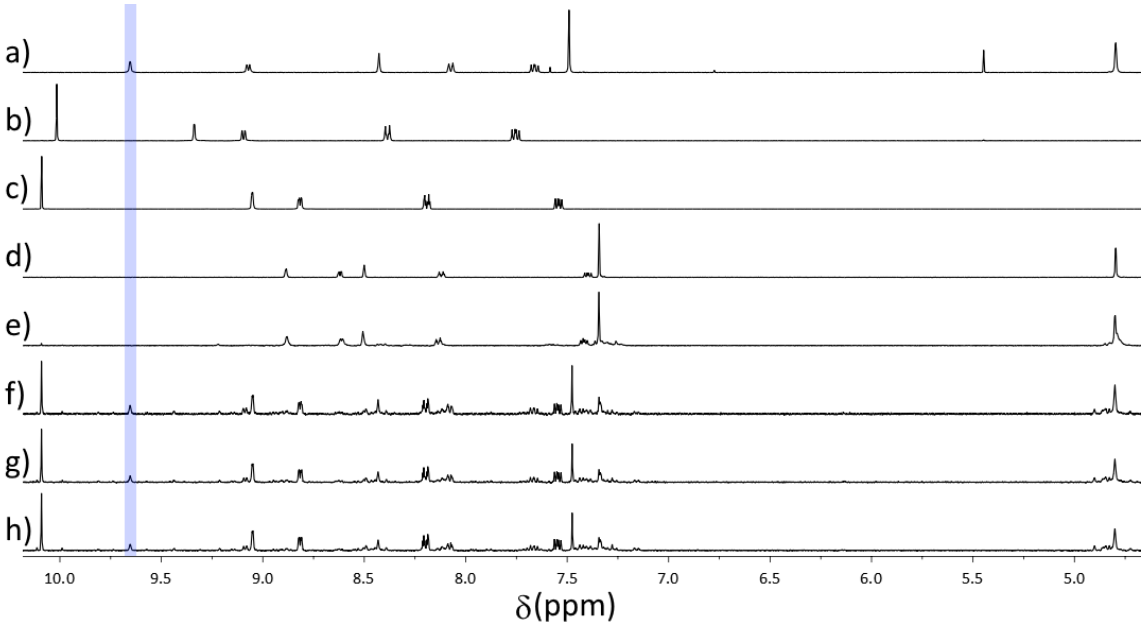

Figure S46: Partial stacked ^{1}H NMR spectra (400 MHz, 298 K, MeCN-d_3) for the attempted formation of $\mathbf{C_{pxy}}$ from its full ligand $\mathbf{L_{pxy}}$; a) $\mathbf{C_{pxy}}$ synthesised using the dynamic covalent approach, b) [Pt(**3-py**)$_4$], c) **3-py**, d) $\mathbf{L_{pxy}}$, e) reaction mixture immediately, f) reaction mixture after 24 h, g) reaction mixture after 48 h, and h) reaction mixture after 72 h. Pale blue highlight designates the ortho proton H_a.

As the precursor complex and subsequent cage are formed under similar conditions to the reaction mixture (60 °C, 18 h), the lack of conversion from the starting materials to the final cage implies that the temperature required for Pt-L ligand exchange/error correction is greatest barrier to forming these cage complexes using the symmetry interaction approach. A higher temperature is required in order to obtain appropriate error correction of the Pt-L bonds. However, that high temperature leads to decomposition/hydrolysis of the imine containing ligands. From the ^{1}H NMR spectra it can be seen that there are a small number of minor peaks the aromatic region, most likely corresponding to kinetically trapped intermediates formed by the ligand and platinum *in situ* that at this temperature are unable to undergo further transformations at useful rates. However, prolonged heating caused the decomposition of the ligand, making it nearly impossible to direct these architectures $[Pt_2L_4]^{4+}$ cage without decomposing it.

6.3 Water stability studies

The stability of the architectures was tested in a 1:1 DMSO-d_6:D_2O solution, whereby saturated solutions of the compounds were created in 300 µL of DMSO-d_6, to which 300 µL of D_2O was added. The solutions were monitored via ^{1}H NMR (400 MHz, DMSO-d_6, 298 K) spectroscopy with spectra recorded at t = 0, 12, 24, 48, 72, 120 and 168 h.

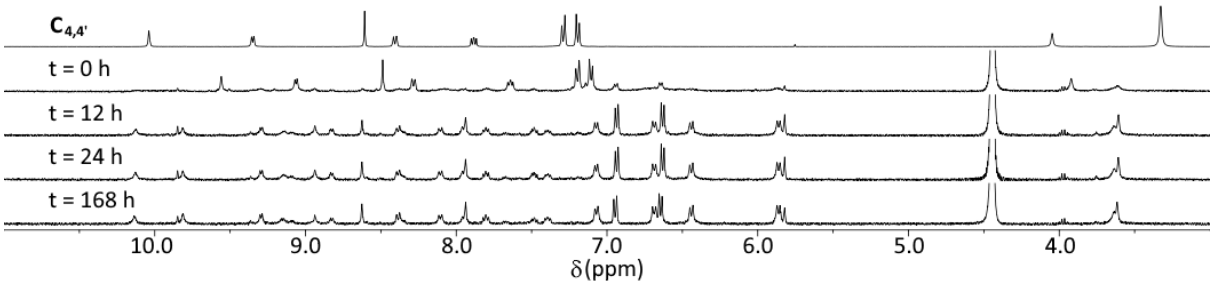

Figure S47: Partial stacked ^{1}H NMR spectra (400 MHz, DMSO-d_6, 298 K) of the decomposition study of **$C_{4,4'}$** in 1:1 DMSO-d_6:D_2O.

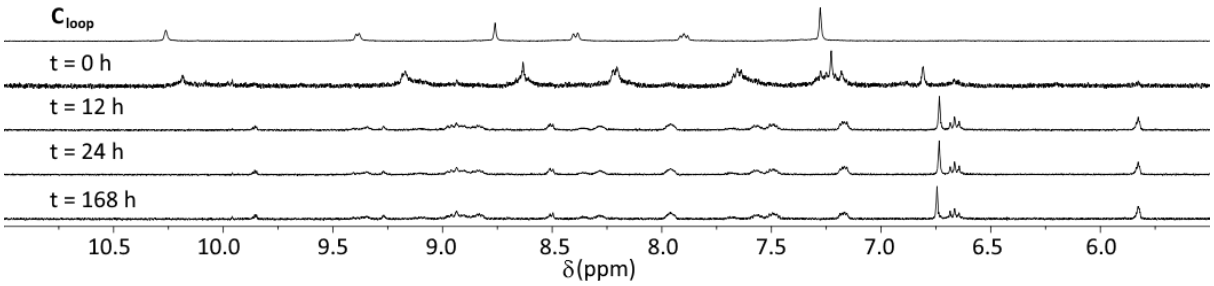

Figure S48: Partial stacked ^{1}H NMR spectra (400 MHz, DMSO-d_6, 298 K) of the decomposition study of **C_{loop}** in 1:1 DMSO-d_6:D_2O.

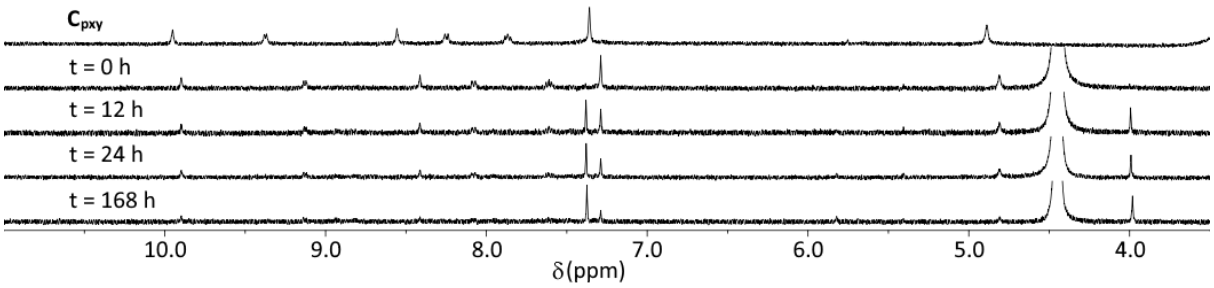

Figure S49: Partial stacked ^{1}H NMR spectra (400 MHz, DMSO-d_6, 298 K) of the decomposition study of **C_{pxy}** in 1:1 DMSO-d_6:D_2O.

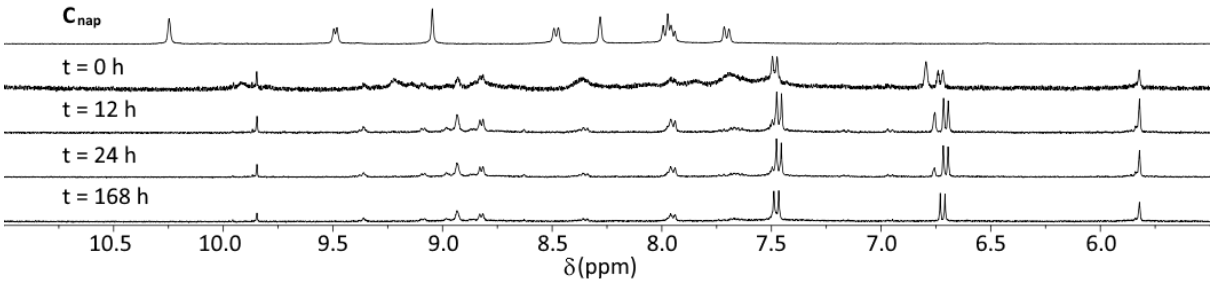

Figure S50: Partial stacked ^{1}H NMR spectra (400 MHz, DMSO-d_6, 298 K) of the decomposition study of $\mathbf{C_{nap}}$ in 1:1 DMSO-d_6:D_2O.

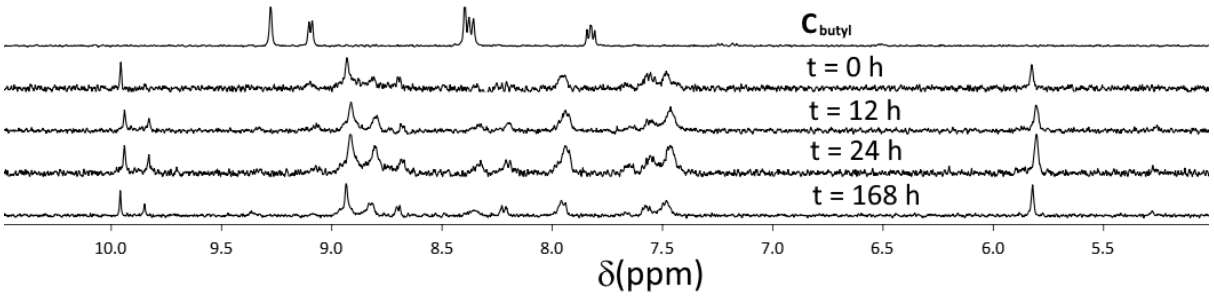

Figure S51: Partial stacked ^{1}H NMR spectra (400 MHz, DMSO-d_6, 298 K) of the decomposition study of $\mathbf{C_{butyl}}$ in 1:1 DMSO-d_6:D_2O.

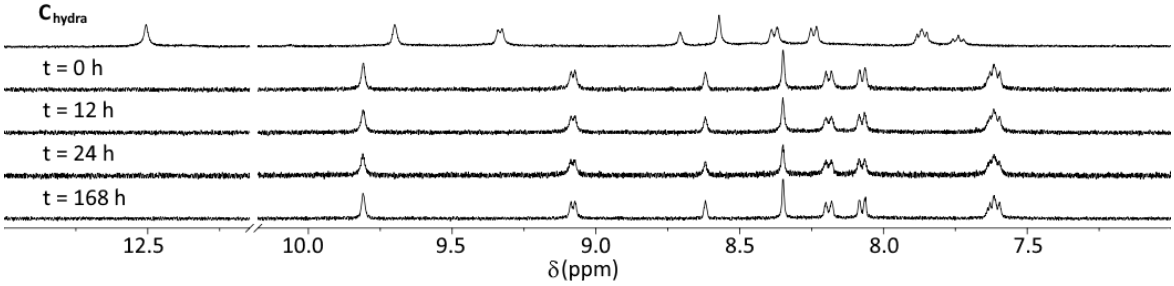

Figure S52: Partial stacked ^{1}H NMR spectra (400 MHz, DMSO-d_6, 298 K) of the decomposition study of $\mathbf{C_{hydra}}$ in 1:1 DMSO-d_6:D_2O.

6.4 Chloride stability studies

The stability of the architectures were tested in the presence of chloride anions, where tetrabutylammonium chloride ([NBu_4]Cl, 10 eq.) was added to a solution of the selected architecture (1 mg) in DMSO-d_6 (0.75 mL). The solutions were monitored via ^{1}H NMR (400 MHz, DMSO-d_6, 298 K) spectroscopy with spectra recorded at t = 0, 1, 12 and 24 h.

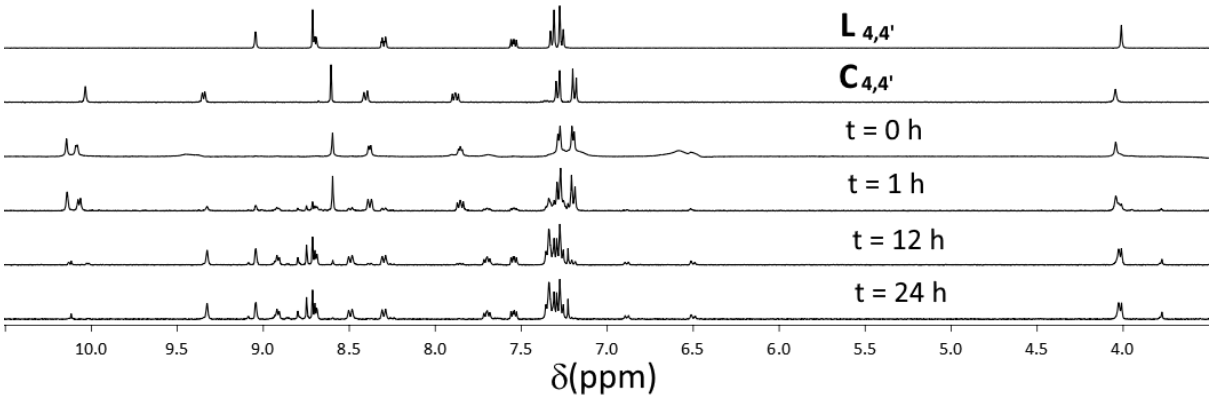

Figure S53: Partial stacked ^{1}H NMR spectra (400 MHz, DMSO-d_6, 298 K) showing the decomposition of $\mathbf{C_{4,4'}}$ over 24 h in the presence of 10 eq. of [NBu_4]Cl.

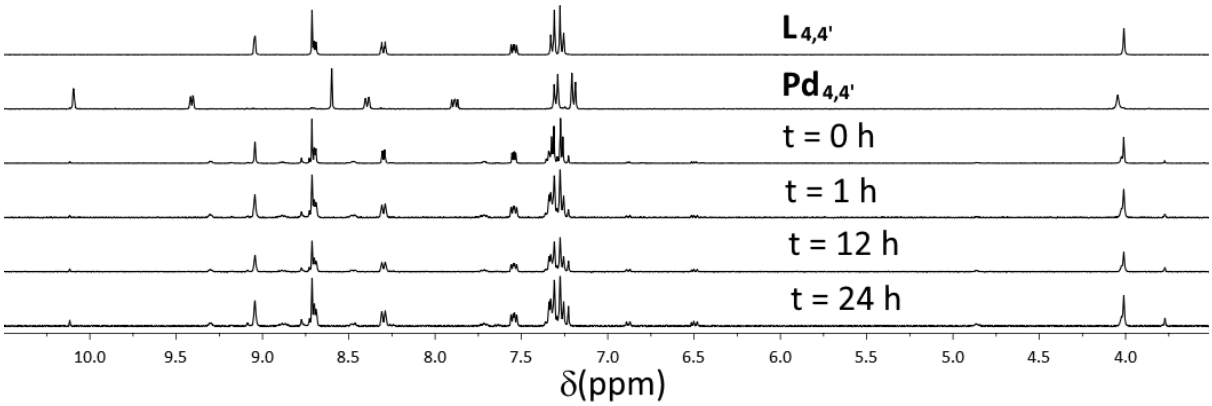

Figure S54: Partial stacked ^{1}H NMR spectra (400 MHz, DMSO-d_6, 298 K) showing the decomposition of $\mathbf{Pd_{4,4'}}$ over 24 h in the presence of 10 eq. of [NBu_4]Cl.

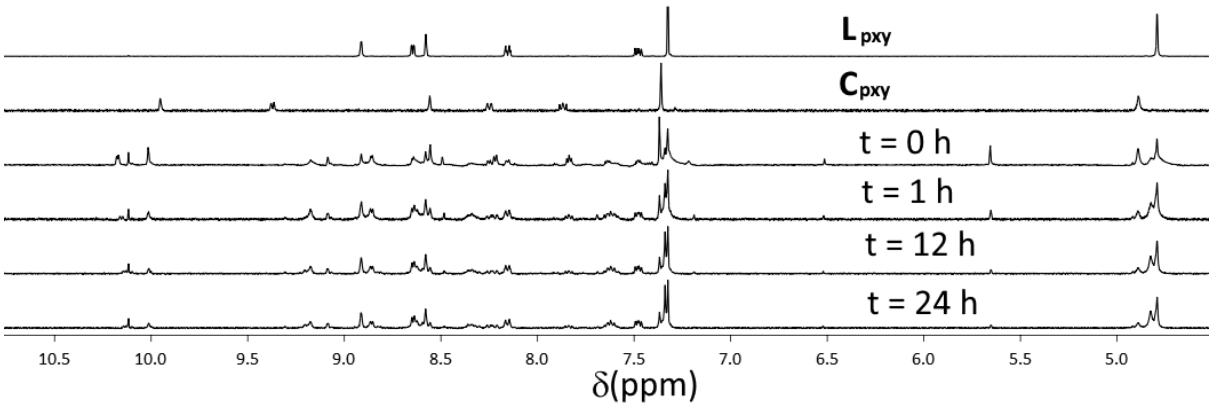

Figure S55: Partial stacked ^{1}H NMR spectra (400 MHz, DMSO-d_6, 298 K) showing the decomposition of $\mathbf{C_{pxy}}$ over 24 h in the presence of 10 eq. of [NBu_4]Cl.

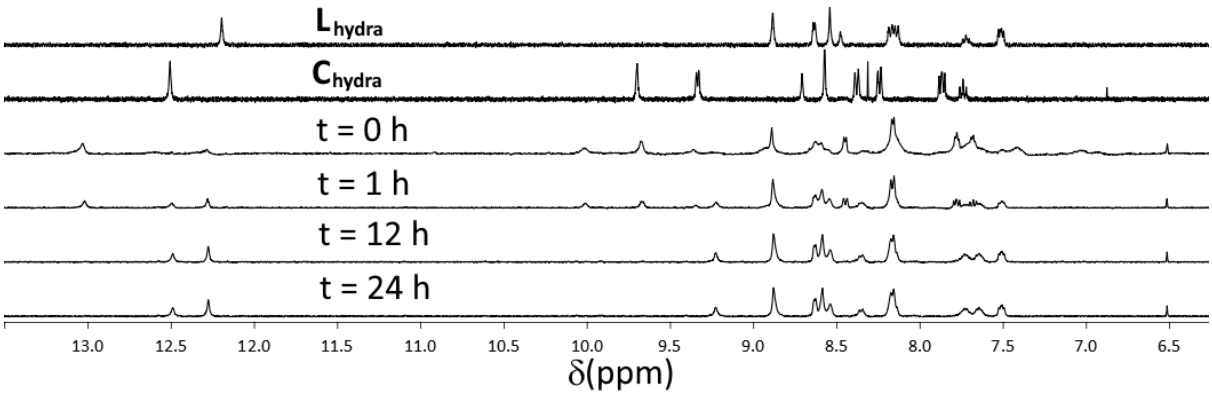

Figure S56: Partial stacked ^{1}H NMR spectra (400 MHz, DMSO-d_6, 298 K) showing the decomposition of $\mathbf{C_{hydra}}$ over 24 h in the presence of 10 eq. of [NBu$_4$]Cl.

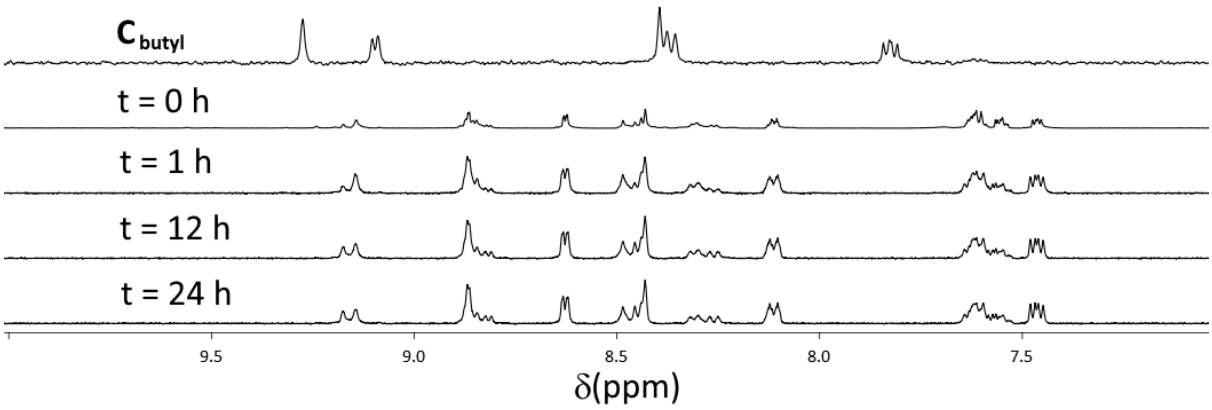

Figure S57: Partial stacked ^{1}H NMR spectra (400 MHz, DMSO-d_6, 298 K) showing the decomposition of $\mathbf{C_{butyl}}$ over 24 h in the presence of 10 eq. of [NBu$_4$]Cl.

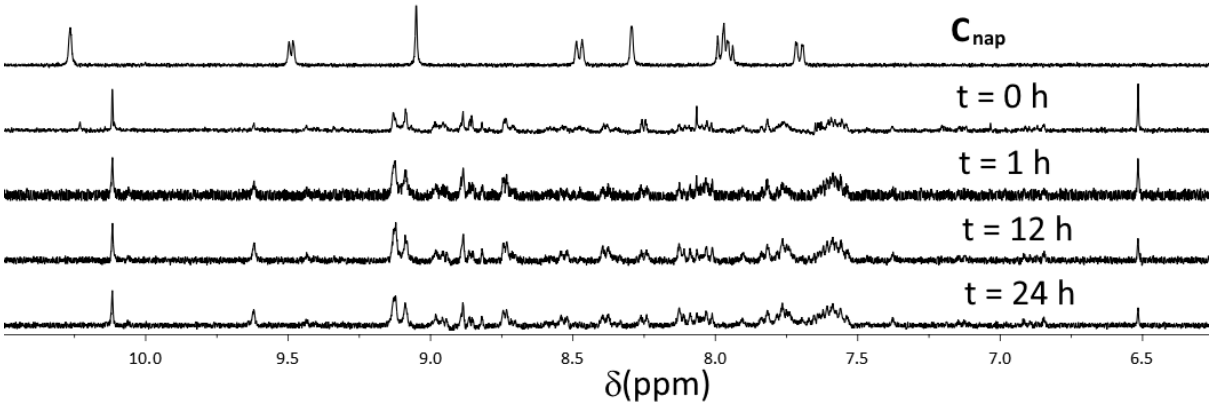

Figure S58: Partial stacked ^{1}H NMR spectra (400 MHz, DMSO-d_6, 298 K) showing the decomposition of $\mathbf{C_{nap}}$ over 24 h in the presence of 10 eq. of [NBu$_4$]Cl.

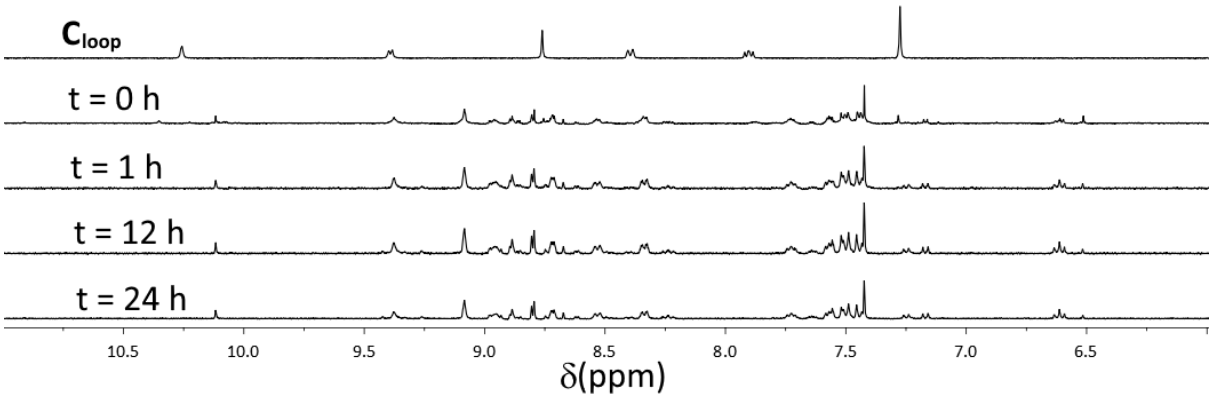

Figure S59: Partial stacked ^{1}H NMR spectra (400 MHz, DMSO-d_6, 298 K) showing the decomposition of $\mathbf{C_{loop}}$ over 24 h in the presence of 10 eq. of [NBu_4]Cl.

6.5 Imine reduction attempts

We attempted to reduce the imine bonds, of the cages, to the corresponding amines to increase the water stability of the architectures. A range of different reducing agents ($NaBH_4$, $NaBH_3CN$, H_3PO_3, Pd/C and H_2, pyridine-BH_3 complex, THF-BH_3 complex or formic acid) were examined, against various $[Pt_2L_4]^{4+}$ cages ($\mathbf{C_{4,4'}}$, $\mathbf{C_{pxy}}$ and $\mathbf{C_{nap}}$). Additionally, a series of different solvents (acetone-d_6, DMSO-d_6, MeCN-d_3, MeOH-d_4) were trialled. The ligands, $\mathbf{L_{4,4'}}$ and $\mathbf{L_{pxy}}$, were reduced *in situ* (in MeCN-d_3 or MeOH-d_4) by addition of excess $NaBH_4$ for ^{1}H NMR spectra comparisons. The cage reductions were attempted in DMSO-d_6 and MeCN-d_3 as these were what the complexes were most soluble in, and methanol-d_4 (MeOH-d_4), as imine reductions are known to progress well in MeOH. Unfortunately, none of the cage reductions proved successful. Initial attempts with $NaBH_4$ and $NaBH_3CN$ seemed to decompose the cages and generate the corresponding free ligand(s), implying they are too harsh to be used in this system.

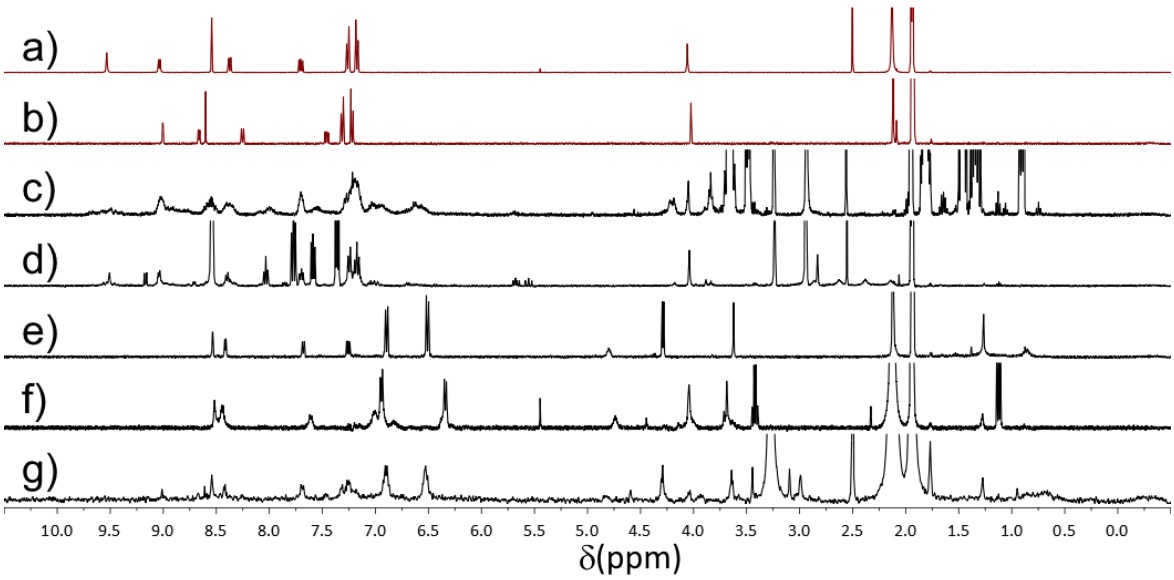

Figure S60: Stacked ^{1}H NMR spectra (400 MHz, MeCN-d_3, 298 K) of the reduction attempts on $\mathbf{C_{4,4'}}$; a) $\mathbf{C_{4,4'}}$, b) $\mathbf{L_{4,4'}}$, c) attempt with BH_3-THF complex, d) attempt with BH_3-pyridine complex, e) reduced $\mathbf{L_{4,4'}}$, f) isolated product reduced $\mathbf{L_{4,4'}}$ from BH_3-pyridine complex attempt and g) attempt with $NaBH_4$.

While the Pd/C hydrogenations did not decompose the cages, the hydrogenation did not occur and returned the initial starting cage under the conditions employed. Reductions with phosphorous acid only returned the starting **3-py** and diamine used as the acidic conditions proved too forceful for the cages and decomposed the imine bonds as well as the platinum(II) complexes. Attempts with BH_3-pyridine complex generated the corresponding reduced free diamine ligands. We suspect due to the excess of pyridine in solution after the reduction the ligand, the pyridine coordinates to the platinum centre and liberates the ligand. The method utilised by Nitschke and co-workers appeared to provide the most success, with the generation of a broad set of signals which may arise from the protons being locked into differing structural conformers upon reduction to the amine, but unfortunately the formation of the product(s) (the amine-containing cages) was unable to be confirmed by ESIMS or HPLC.

6.6 ^{19}F NMR spectra

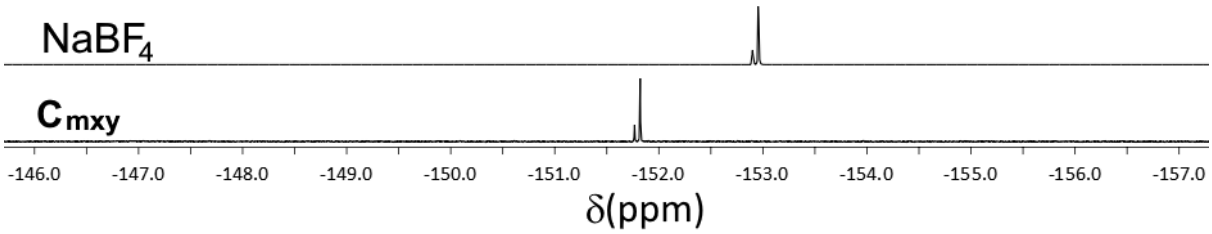

Figure S61: Partial stacked ^{19}F NMR spectra (376 MHz, MeCN-d_3, 298 K) showing the fluorine environments of $NaBF_4$ and $\mathbf{C_{mxy}}$.

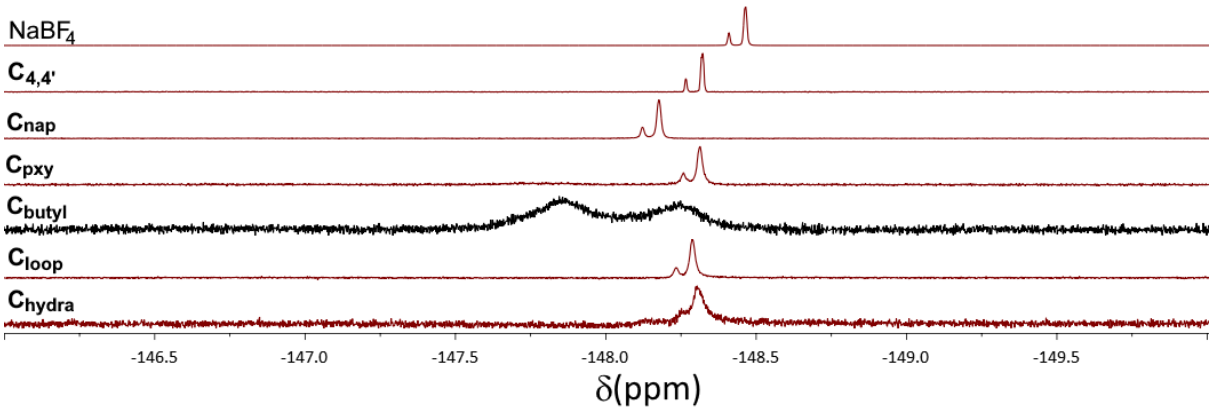

Figure S62: Partial stacked ^{19}F NMR spectra (376 MHz, DMSO-d_6, 298 K) showing the fluorine environments of $NaBF_4$ and $\mathbf{C_{4,4'}}$, $\mathbf{C_{nap}}$, $\mathbf{C_{pxy}}$, $\mathbf{C_{butyl}}$, $\mathbf{C_{loop}}$ and $\mathbf{C_{hydra}}$.

6.7 Host-guest studies

Host-guest (HG) studies were performed on the architectures $\mathbf{C_{4,4'}}$, $\mathbf{C_{loop}}$, $\mathbf{C_{pxy}}$, $\mathbf{C_{nap}}$, and $\mathbf{C_{hydra}}$. Due to the low solubility of $\mathbf{C_{butyl}}$ it was excluded from the HG screening experiments. $\mathbf{C_{hydra}}$ was only screened in DMSO-d_6 due to its insolubility in MeCN-d_3. The corresponding host (0.5 mg) and guest were combined in DMSO-d_6 (0.5 mL) or MeCN-d_3 (0.5 mL) in a 1.0/1.0 or a 1.0/4.0 eq. ratio respectively, and their ^{1}H NMR spectra (400 MHz, 298 K) were investigated for shifts in the proton environments.

Table S2: Host-guest adduct formation studies. Host environments: * denotes the inwardly pointing ortho proton to the endocyclic N atom on the coordinated pyridine ring. • denotes the outwardly pointing ortho proton on the coordinated pyridine ring. ▪ denotes the protons on the phenyl ring.

Architecture	Guest	Solvent	Signal	Shift in Signal
$C_{4,4'}$	Carmustine	MeCN	*	0.02
	Cyclophosphamide	MeCN	*	0.02
	Temozolomide	MeCN	*	0.01
C_{loop}	1,2-Diaminoanthraquinone	MeCN	*	0.27
	6,13-Pentacenequinone	DMSO	•	-0.07
C_{pxy}	1,4-Dimethylanthraquinone	MeCN	▪	-0.02
	Busulfan	MeCN	*	0.06
	Temozolomide	MeCN	*	0.06
C_{nap}	1,4-Benzoquinone	MeCN	*	-0.01
	N,N'-Trimethyleneurea	MeCN	*	-0.01
	9,10-Anthraquinone	MeCN	▪	-0.02
	1,2-Diaminoanthraquinone	DMSO	▪	-0.02
	2,6-Diaminoanthraquinone	DMSO	▪	-0.02
	6,13-Pentacenequinone	DMSO	▪	-0.02
	1,4-Dimethylanthraquinone	MeCN	▪	-0.02
	Busulfan	MeCN	*	-0.02
	Temozolomide	MeCN	▪	-0.06
	Carboplatin	DMSO	▪	-0.03
	Cinoxacin	MeCN	*	0.03
	Nalidixic acid	MeCN	*	0.01
C_{hydra}	6,13-Pentacenequinone	DMSO	*	-0.07

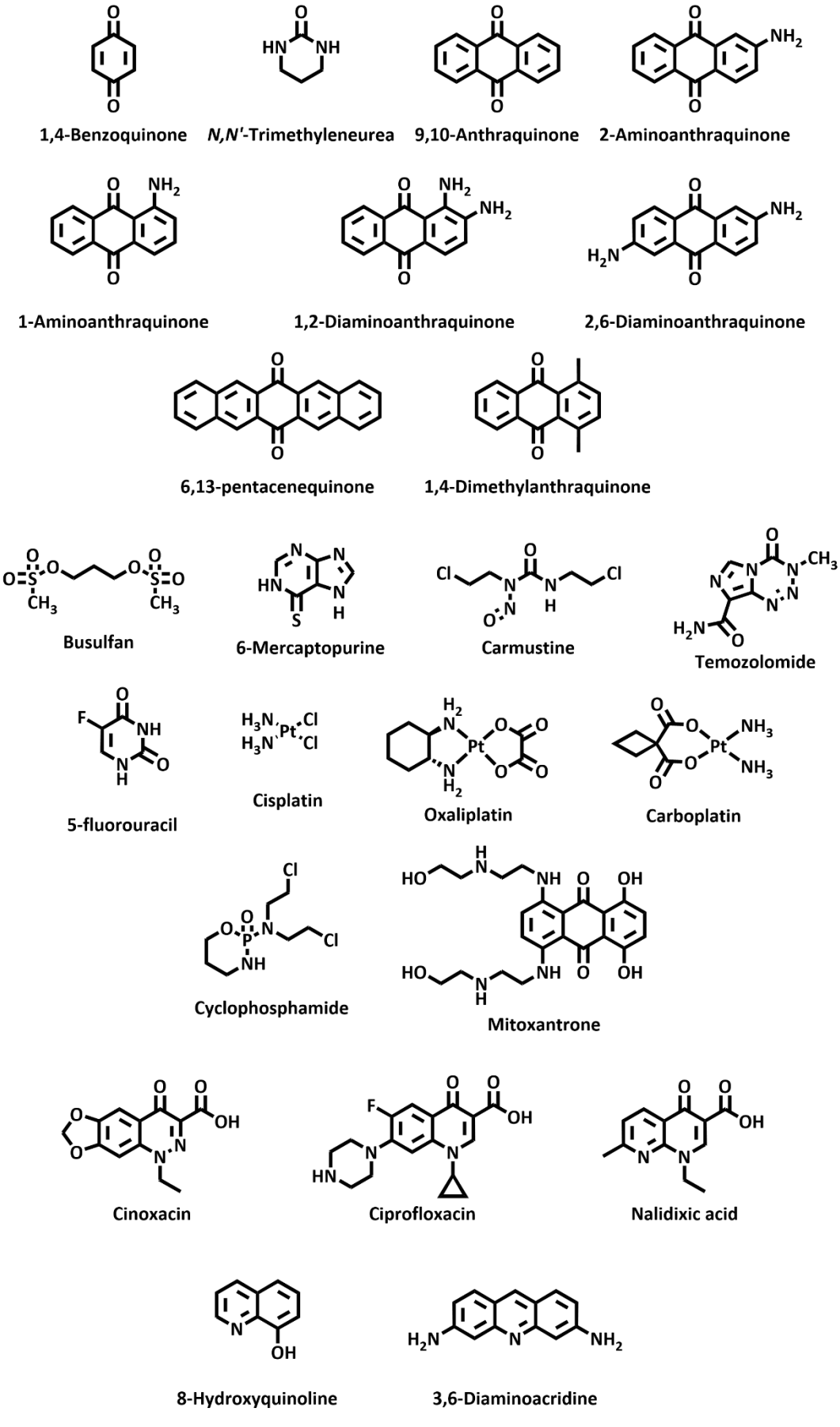

Figure 63: Chemical structures of screened guests.

7 SPARTAN'16® MMFF models

Spartan models were generated using SPARTAN'16® and minimized using the Merck Molecular Force Field (MMFF).

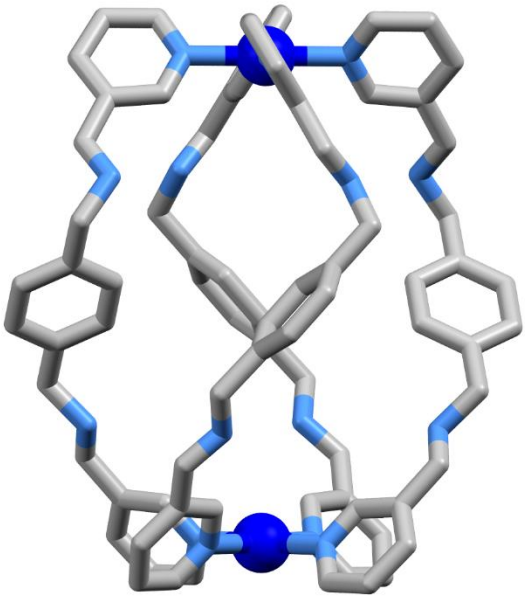

Figure S64: SPARTAN'16® MMFF model of $\mathbf{C_{pxy}}$. Hydrogen atoms were omitted for clarity.

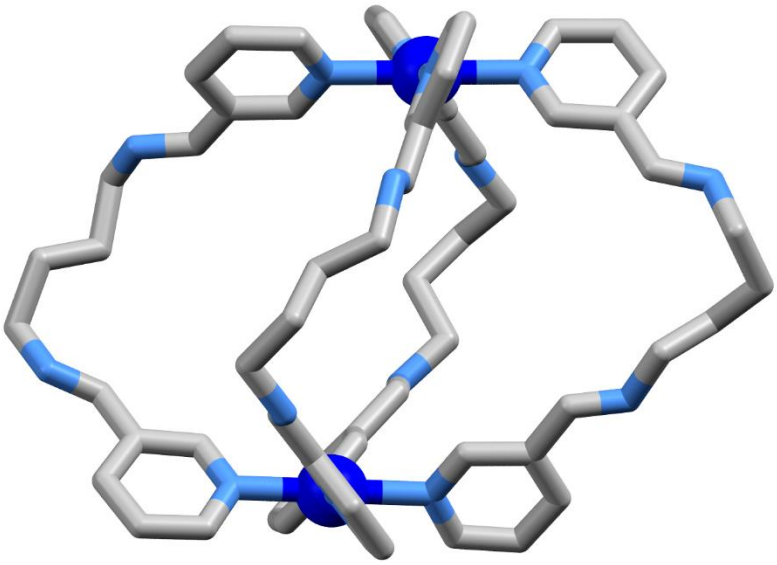

Figure S65: SPARTAN'16® MMFF model of $\mathbf{C_{butyl}}$. Hydrogen atoms were omitted for clarity.

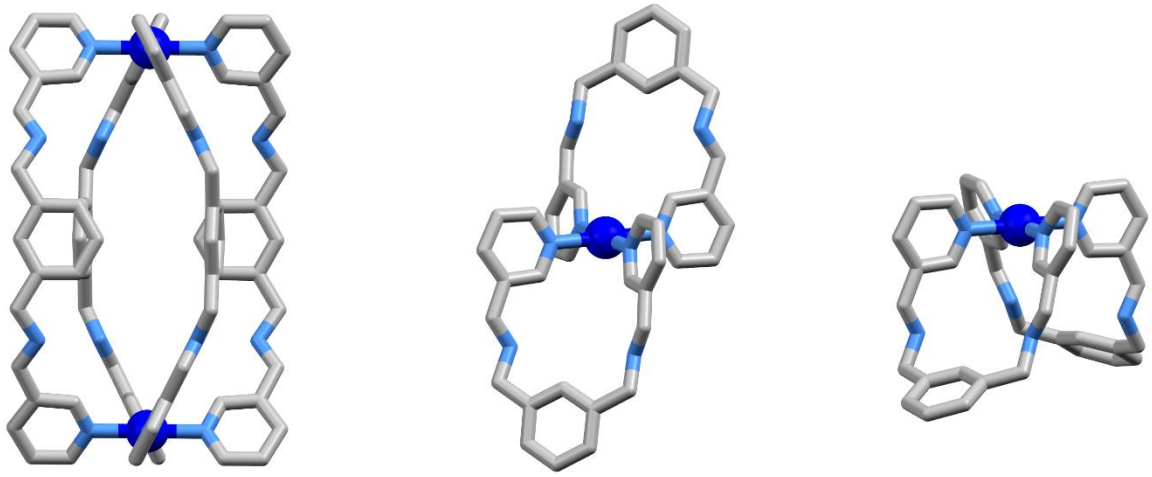

Figure S66: SPARTAN'16® MMFF models of initial presumed $\mathbf{C_{mxy}}$ cage (left) and potential structures of $\mathbf{C_{mxy}}$ complex (middle and right). Hydrogen atoms were omitted for clarity.

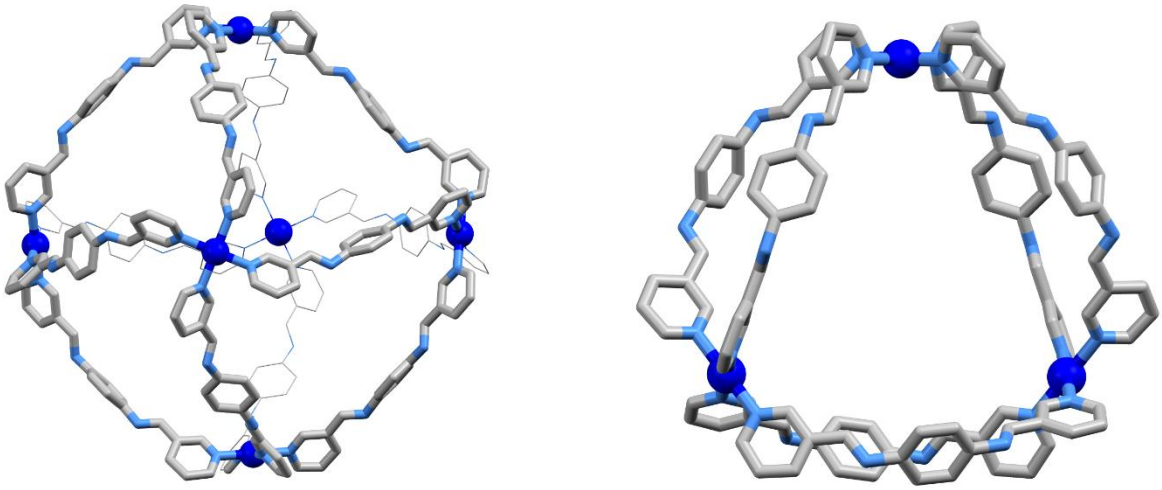

Figure S67: SPARTAN'16® MMFF models of initial presumed $\mathbf{C_{oct}}$ octahedron (left) and proposed structure of $\mathbf{C_{loop}}$ double walled triangle (right). Hydrogen atoms were omitted for clarity.

8 Molecular Structures

X-ray data was collected at 100 K on an Agilent Technologies Supernova system using Cu Kα radiation with exposures over 1.0°, and the data were treated with CrysAlisPro software. The structure was solved using SHELXT within OLEX2 and weighted full matrix refinement F^2 was performed using SHELXL-97 running within the OLEX2 package.[9] All non-hydrogen atoms were refined anisotropically, with hydrogen atoms attached to carbons placed in calculated positions and refined using a riding model. Ellipsoids are shown at 50% probability level.

8.1 $C_{4,4'}$

CCDC#: 2320665. X-ray structural data for **$C_{4,4'}$** were collected from light green prism-shaped crystals that were grown via the vapor diffusion of diethyl ether into a concentrated solution of the cage in nitromethane. The structure was solved in the triclinic space group *P*-1 and refined to an R_1 value of 6.87%. The asymmetric unit contains two of the ligands **$L_{4,4'}$**, a single platinum metal ion and two BF_4^- counterions. A "solvent mask" (OLEX2 package) was applied to resolve diffused electron density within the lattice which could not be appropriately modelled, where a void consisting of 210 electrons in the unit cell was attributed to approximately 6 nitromethane solvent molecules (6 × 32 electrons = 192 electrons) with the presence of some diethyl ether unable to be discounted. Void content was not included in the chemical formulae. One of the BF_4^- counterions was disordered. This was addressed through use of the SADI and ISOR commands. The cif check gave two B alerts, PLAT971 and PLAT972, regarding residual density near the platinum(II) metal ion. This presumably arises from problems with absorption corrections near the heavy metal. Connectivity is in any case clear for the cationic structure.

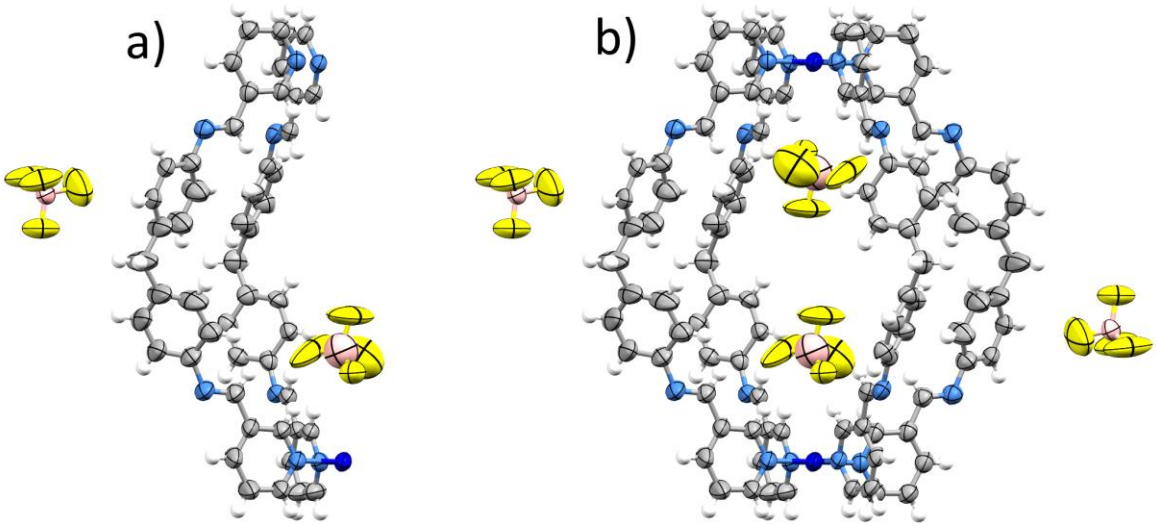

Figure S68: a) Mercury ellipsoid plot of the asymmetric unit of $\mathbf{C_{4,4'}}$ and b) full $[Pt_2L_4](BF_4)_4$ structure of $\mathbf{C_{4,4'}}$.

8.2 $\mathbf{C_{nap}}$

CCDC#: 2320664. X-ray structural data for $\mathbf{C_{nap}}$ were collected from light yellow plate-shaped crystals that were grown via the vapour diffusion of diethyl ether into a concentrated solution of the cage in nitromethane. The structure was solved in the monoclinic space group *C*2/m and refined to an R_1 value of 5.1%. The asymmetric unit contains one of the ligands and a single platinum metal ion. There was residual electron density within the lattice (754 electrons per unit cell) that could not be appropriately modelled. A "solvent mask" (OLEX2 package) was applied to resolve this problem. We attribute this density to BF_4^- counterions ((8 x 41 electrons = 328 electrons) and nitromethane solvent (approx. 13 x 32 electrons = 416 electrons). Fifteen reflections were omitted as they had error/esd values >|5|. There were no A or B alerts for this structure.

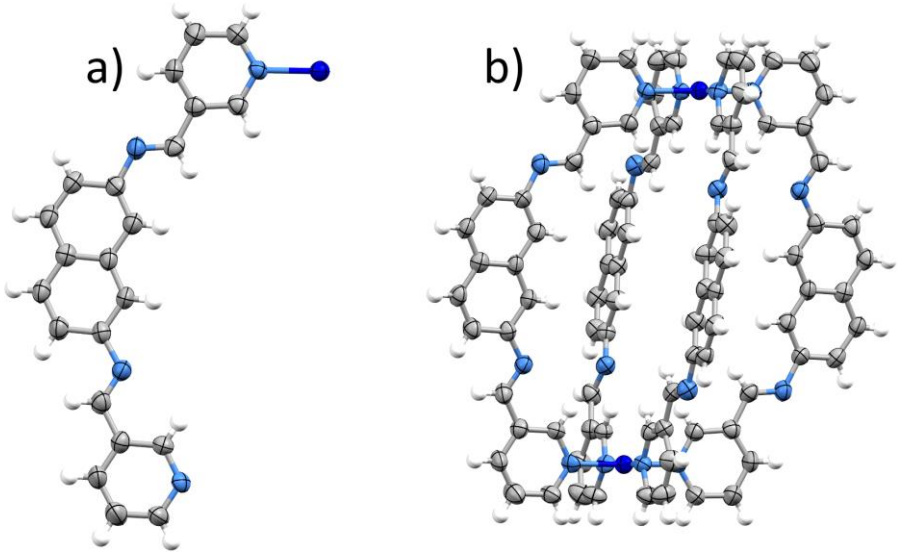

Figure S69: a) Mercury ellipsoid plot of the asymmetric unit of **C_{nap}**, and b) full $[Pt_2L_4]^{4+}$ structure of **C_{nap}**.

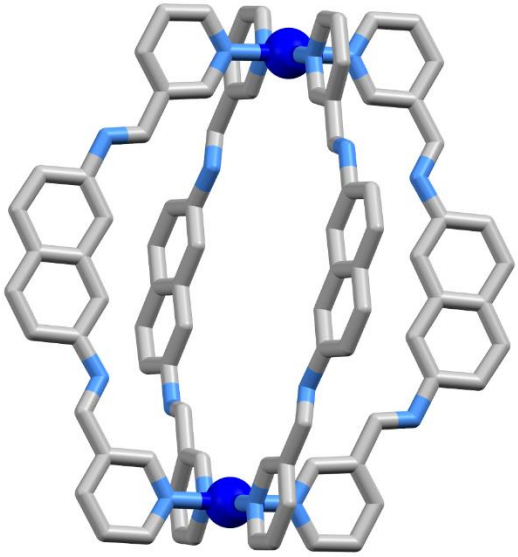

Figure S70: X-ray crystal structure of **C_{nap}**. Hydrogen atoms were omitted for clarity.

	$C_{4,4'}$		C_{nap}	
CCDC#	2320665		2320664	
Empirical formula	$C_{100}H_{80}B_4F_{16}N_{16}Pt_2$		$C_{88}H_{64}N_{16}Pt_2$	
Formula weight	2243.22		1735.73	
Temperature/K	100.01 (10)		100.01 (10)	
Crystal system	Triclinic		Monoclinic	
Space group	*P*-1		*C*2/m	
Unit cell dimensions	a/Å = 11.1598 (4)	α/° = 87.192 (3)	14.2019 (9)	90
	b/Å = 14.8934 (5)	β/° = 75.514 (3)	21.4417 (13)	98.888(7)
	c/Å = 17.8869 (6)	γ/° = 86.266 (3)	19.1515 (13)	90
Volume/Å^3	2870.67 (18)		5761.8 (6)	
Z	1		2	
ρ_{calc} g/cm^3	1.298		1.000	
μ/mm^{-1}	5.112		4.774	
F(000)	1112.0		1720.0	
Crystal size/mm^3	0.283 × 0.249 × 0.201		0.159 × 0.088 × 0.029	
Radiation/Å	Cu Kα (λ = 1.54184)		Cu Kα (λ = 1.54184)	
2Θ range for data collection/°	7.71 to 145.552		9.348 to 145.452	
Index ranges	-13 ≤ h ≤ 13, -18 ≤ k ≤ 18, -21 ≤ l ≤ 22		-17 ≤ h ≤ 12, -26 ≤ k ≤ 21, -23 ≤ l ≤ 21	
Reflections collected	42580		11232	
Independent reflections	11226 [R_{int} = 0.0617, R_{sigma} = 0.0437]		5690 [R_{int} = 0.0793, R_{sigma} = 0.1076]	
Data/restraints/parameters	11226/111/622		5690/0/241	
Goodness-of-fit on F^2	1.070		0.904	
Final R indexes [I>=2σ (I)]	R_1 = 0.0687, wR_2 = 0.1887		R_1 = 0.0509, wR_2 = 0.1078	
Final R indexes [all data]	R_1 = 0.0805, wR_2 = 0.1998		R_1 = 0.0713, wR_2 = 0.1175	
Largest diff. peak/hole / e Å^{-3}	2.56/-2.64		0.96/-1.06	

9 References

1. a) G. S. Huff, W. K. C. Lo, R. Horvath, J. O. Turner, X.-Z. Sun, G. R. Weal, H. J. Davidson, A. D. W. Kennedy, C. J. McAdam, J. D. Crowley, M. W. George and K. C. Gordon, *Inorg. Chem.*, 2016, **55**, 12238-12253; b) P. Van Thong, D. T. Thom and N. T. T. Chi, *Vietnam J. Chem.*, 2018, **56**, 146-151.
2. a) A. Jerschow and N. Müller, *J. Magn. Reson.*, 1997, **125**, 372-375; b) A. Jerschow and N. Müller, *Journal of Magnetic Resonance, Series A*, 1996, **123**, 222-225.
3. S. N. Ignat'eva, A. S. Balueva, A. A. Karasik, D. V. Kulikov, A. V. Kozlov, S. K. Latypov, P. Lönnecke, E. Hey-Hawkins and O. G. Sinyashin, *Russ. Chem. Bull.*, 2007, **56**, 1828-1837.
4. R. A. Fernandes and J. L. Nallasivam, *ChemistrySelect*, 2020, **5**, 8301-8304.
5. A. Y. Chen, P. W. Thomas, A. C. Stewart, A. Bergstrom, Z. Cheng, C. Miller, C. R. Bethel, S. H. Marshall, C. V. Credille, C. L. Riley, R. C. Page, R. A. Bonomo, M. W. Crowder, D. L. Tierney, W. Fast and S. M. Cohen, *J. Med. Chem.*, 2017, **60**, 7267-7283.
6. H. H. Eissa, *Org. Chem. Curr. Res*, 2015, **4**, 151-163.
7. L. S. Lisboa, J. A. Findlay, L. J. Wright, C. G. Hartinger and J. D. Crowley, *Angew Chem Int Ed Engl*, 2020, **59**, 11101-11107.
8. S. Bandi and D. K. Chand, *Chem. Eur. J.*, 2016, **22**, 10330-10335.
9. a) G. Sheldrick, *Acta Crystallogr. Section A*, 2008, **64**, 112-122; b) O. V. Dolomanov, L. J. Bourhis, R. J. Gildea, J. A. K. Howard and H. Puschmann, *J. Appl. Crystallogr.*, 2009, **42**, 339-341.